indicate that aPKC specifically phosphorylates HIV-1 Gag at Ser487 both *in vitro* and *in vivo*.

### The phosphorylation of Gag Ser487 facilitates the interaction between Gag and Vpr

HIV-1 Gag p6 contains a late domain consisting of three protein binding motifs, PTAP (Tsg101 binding), LYPXnL (Alix binding) and C-terminal Vpr. Ser487 is located in the Alix binding motif and is also adjacent to the Vpr binding motif spanning amino acids 488–492 (Figure 4A). To obtain structural-based information on Gag phosphorylation on Ser487 and how it affects the interaction of Gag with Alix or Vpr, we conducted computer-assisted molecular modeling of the Gag p6 domain coupled with peptides derived from either Alix or Vpr. The models constructed in this study included unphosphorylated and phosphorylated Gag-p6 (amino acids Tyr483-Ser494), and its Ser/Ala substituted mutant on Ser487 (S487A). Molecular modeling calculations with thermodynamically optimized three dimensional structures showed less than 1 Å of positional shifts of Cα atoms of Gag-p6 by phosphorylation, suggesting no obvious difference in the basic structure of Gag-p6 irrespective of the phosphorylation status. Furthermore, binding interface between Gag-p6 and Alix was not affected by the phosphorylation (Figure 4B, Upper panels) or Ser/Ala substitution of Gag Ser487 [31-33]. On the other hands, the binding of Gag-p6 with Vpr was facilitated since the phosphorylation of Ser487 can create another hydrogen bond between Gag-p6 and Vpr (Figure 4B, Lower panels). The Ser487 was predicted to form no hydrogen bonds with Vpr in non-phosphorylated state, whereas the phosphorylated Ser487 could form the hydrogen bond with Gln44 of Vpr. Consequently, binding energy calculated with Molecular Operating Environment (MOE) was significantly increased by phosphorylation of Ser487 only for the Gag-p6-Vpr complex (Figure 4B, tables). These data suggest that the phosphorylation of Gag-p6 on Ser487 could indeed affect the binding affinity of Gag-p6 with Vpr but not Alix.

Based on our structural modeling results, we next asked whether the phosphorylation of Gag at Ser487 has

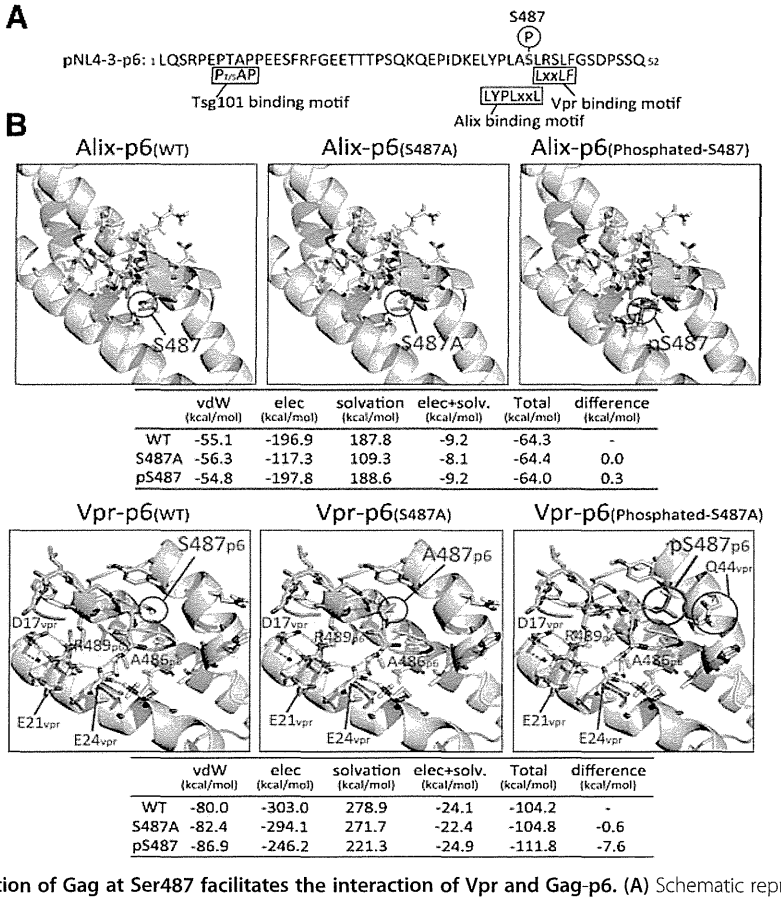



**Figure 4 The phosphorylation of Gag at Ser487 facilitates the interaction of Vpr and Gag-p6. (A)** Schematic representation of the HIV-1 Gag-p6 sequence indicating the binding motifs, Tsg101, Alix and Vpr, located around the Ser487 site. **(B)** Complex structure models of Gag-p6 with Alix or Vpr. The structural calculations were undertaken using MOE. Upper panel shows structural models of the interaction of Alix with wild-type Gag-p6, Gag-p6Ser487A or phosphorylated Gag-p6-Ser487. Bottom panel shows structural models of the interaction of Vpr with wild-type Gag-p6, Gag-p6Ser487A or phosphorylated Gag-p6-Ser487. Binding energies of p6 with Alix or Vpr calculated from the structural models were shown in the bottom tables, where the highly negative value indicates the stable binding.

any effect on the interaction between Vpr and Gag. We have selected Bimolecular Fluorescence Complementation (BiFC) system to quantify the Vpr-Gag interaction in live cells as previously reported [34]. Plasmids encoding C-terminally KGC-tagged Gag (Gag-KGC) and N-terminally KGN-tagged Vpr (KGN-Vpr) were transfected and evaluated for BiFC signal by flow cytometry (Figure 5A). Flow cytometry analysis revealed that the interaction of Vpr with Gag-Ser487Ala mutant was reduced as compared with wild-type Gag (Figure 5A). To further assess whether the phosphorylation of Gag at Ser487 provides another hydrogen bond with Vpr Gln44 to facilitate Gag-

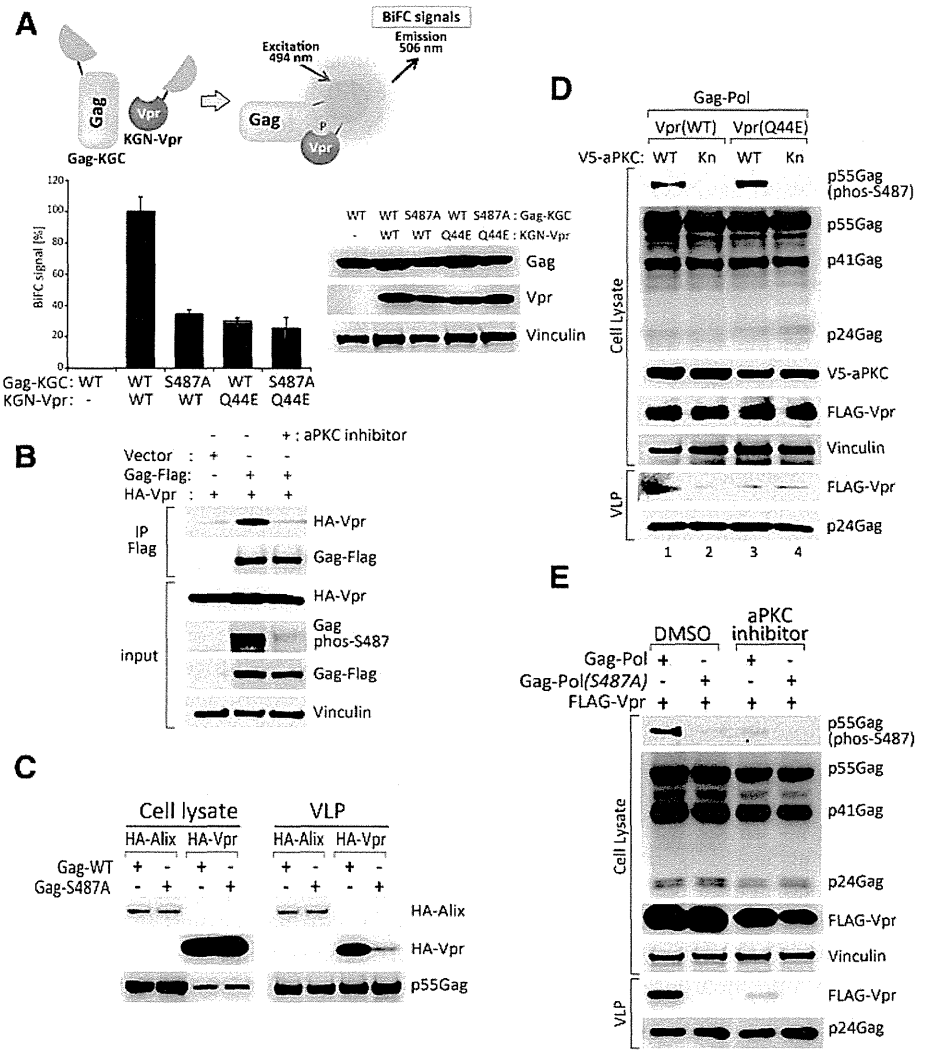



**Figure 5 The phosphorylation of Gag at Ser487 promotes the incorporation of Vpr into HIV-1 virions. (A)** Bimolecular fluorescence complementation (BiFC) of 293T cells expressing Gag-KGC and KGN-Vpr (upper panel). 293T cells were transfected with KGN-Vpr (WT or Q44E) and Gag-KGC or Gag (S487A)-KGC, were harvested and analyzed by flow cytometry to determine the BiFC signal at 48 hours post-transfection. Results represent the means of three independent experiments. The cells were harvested and subjected to western blot analysis. **(B)** The phosphorylation of Gag at Ser487 promotes interaction of Vpr with Gag. HA-tagged Vpr was co-transfected with Flag tagged Gag into 293T cells in presence of 5 μM aPKC inhibitor or DMSO, followed by pulldown with Flag-beads and immunoblotting with indicated antibodies. Bottom panel shows input for pulldown assay. **(C)** Differential effect of Gag Ser487 phosphorylation on Alix and Vpr incorporation into VLPs. 293T cells were transfected with GFP-tagged Gag (Gag-WT) or with the Ser487 point mutated Gag (Gag-S487A), with either HA-tagged Alix, or HA-tagged Vpr expression vectors. Cells and VLPs were collected at 24 hours post-transfection, and their protein extracts were resolved using SDS-PAGE and subjected to western blot analysis. **(D)** aPKC-mediated Gag phosphorylation at Ser487 facilitates Vpr incorporation into virions. 293T cells were transiently transfected with Gag-Pol, either Flag-tagged Vpr (WT) or Gln44 point mutated Vpr (Q44E), and with either V5-tagged aPKC (WT) or kinase-negative aPKC (Kn). Cell lysates and VLPs were collected 24 hours post-transfection and subjected to western blot analysis. **(E)** The phosphorylation of Gag-pol-Ser487 is required for Vpr incorporation into HIV-1 virions. 293T cells were transfected with Flag-tagged Vpr and either with Gag-Pol (WT) or with the Ser487 point mutated Gag-Pol (S487A). The transfected 293T cells were treated with DMSO or aPKC inhibitor for 24 hours. Cell lysates and VLPs were collected and subjected to western blot analysis.

Vpr interaction, we constructed Vpr Q44E mutant for BiFC analysis. Results demonstrated that Vpr Q44E mutant exhibited weker interactions to Gag and Gag S487A as compared with wild type Vpr (Figure 5A). We further found that aPKC inhibitor suppressed the interaction between Gag-Flag and HA-Vpr in imunoprecipitation analysis (Figure 5B).

### The phosphorylation of Gag at Ser487 affects Vpr incorporation into virions and viral infectivity

We next examined whether the phosphorylation of Gag at Ser487 has any effects on the incorporation of Vpr into HIV-1 virus like particles (VLP). As shown in Figure 4B, we found no distinct changes in the incorporation of Alix into VLPs regardless of a Ser/Ala substitution at Gag Ser487 in 293T cells. However, Vpr incorporation into VLP was significantly decreased in cells transfected with the Gag-Ser487Ala mutant as compared with cells transfected with wild-type Gag (Figure 5C). Hence, it is plausible that the phosphorylation of Gag at Ser487 may have an important role in its interaction with Vpr thereby affecting the Vpr incorporation into VLPs.

To further explore the relevance of Gag phosphorylation to HIV-1 replication, we examined whether aPKC kinase activity is necessary to regulate Vpr incorporation into HIV-1 virions. Gag phosphorylation at Ser487 was prominently enhanced by wild type aPKC but not kinase negative mutant aPKC (Kn) (Figure 5D). Concomitantly, the level of Vpr incorporation into virions was shown to be paralleled with the Gag phosphorylation status (lane 1 and 2 in Figure 5D). More importantly, virion incorporation of Vpr Q44E mutant was much lesser than wild-type Vpr irrespective of Gag phosphorylation at Ser487 (lane3 and 4 in Figure 5D). These results suggest that Gag phosphorylation at Ser487 is indeed affect Vpr incorporation and this process could be mediated by the Gln44 residue of Vpr. Although no significant effect of the Gag-pol S487A mutant on the Vpr expression levels in cells was evident, the Vpr incorporation level into VLPs was significantly reduced upon Gag-pol-S487Ala transfection (Figure 5E). Consistent with this result, the incorporation of Vpr into VLPs was significantly reduced in cells treated with the aPKC inhibitor peptide; the Vpr incorporation efficiency was reduced in aPKC inhibitor treated cells (Figure 5E). These data indicate that aPKC can enhance the incorporation of Vpr into HIV-1 virions.

It has been well established that Vpr incorporation into HIV-1 virions augments viral infectivity in macrophages [5,6,35-37]. We thus assessed whether aPKC affects HIV-1 infectivity by increasing Vpr incorporation into virions. We hypothesized that if the Gag phosphorylation at Ser487 by aPKC was beneficial for HIV-1 infection in this way, aPKC activity would affect wild type HIV-1 but not a Vpr-null virus. To test this, we employed pNL4-3ΔEnv-luc (WT) or pNL4-3ΔEnvΔVpr-luc (Vpr-null) strains. We then produced the corresponding viruses with a fusiogenic envelope G glycoprotein of the vesicular stomatitis virus (VSV-G) in the presence or absence of aPKC inhibitor in 293T cells (Figure 6A). Immunoblotting analysis of VLP demonstrated that the level of Vpr incorporation was prominently reduced by treatment with the aPKC peptide inhibitor (Figure 6B). The infectivity of the generated viruses was tested using the human monocyte/macrophage cell line MonoMac6. The aPKC inhibitor-treated WT virus exhibited approximately 50% less infectivity than the control WT virus (Figure 6C). The Vpr-null virus showed a 35% reduction in infectivity compared with the WT virus in the MonoMac6 cells (Figure 6C). However, the primarily low infectivity of the Vpr-null virus was not significantly affected by the aPKC inhibitor (Figure 6C). aPKC inhibitor did not exhibit obvious cytotoxic effect to MonoMac 6 cells (Figure 6D).

To assess the role of aPKC in multi-round HIV-1 replication in primary monocyte-derived macrophages (MDMs), we infected these cells with HIV-$1_{89.6}$, a dual tropic virus, or HIV-$1_{NLAD8}$, an R5 tropic virus, in conjunction with treatments of various concentrations of the aPKC inhibitor (Figure 7A). The results revealed that the aPKC inhibitor strongly suppressed the replication of both viruses in a dose-dependent manner (Figure 7B, C), although there was no obvious toxicity or growth inhibition in these cells (Figure 7D). Taken together, these results indicate that the phosphorylation of Gag by aPKC regulates Vpr incorporation and HIV-1 replication in macrophages.

## Discussion

We here demonstrate that aPKC is a crucial regulator of HIV-1 infection via the phosphorylation of Gag-p6 which enhances the incorporation of Vpr into virions. Our current data strongly suggest that Ser487 is the specific phosphorylation site on HIV-1 Gag for aPKC and is crucial for the Gag p6-Vpr interaction that leads to Vpr incorporation into viral particles. Furthermore, our current data demonstrate that an aPKC inhibitor prominently inhibits HIV-1 replication in primary human macrophages. Hence, the phosphorylation of Gag by aPKC may well be an important mechanism through which HIV-1 efficiently infects macrophages and by which an excessive accumulation of the cytotoxic Vpr protein in the host infected cells is prevented.

The Gag-p6 domain has been identified as the predominant site of phosphorylation in HIV-1 particles [22]. Ser487 is a highly conserved residue in this p6 domain among various HIV-1 strains, suggesting that the phosphorylation of this residue is of fundamental functional importance. Votteler et al. have demonstrated that a HIV-1 Gag mutant with a deleted PTAP region

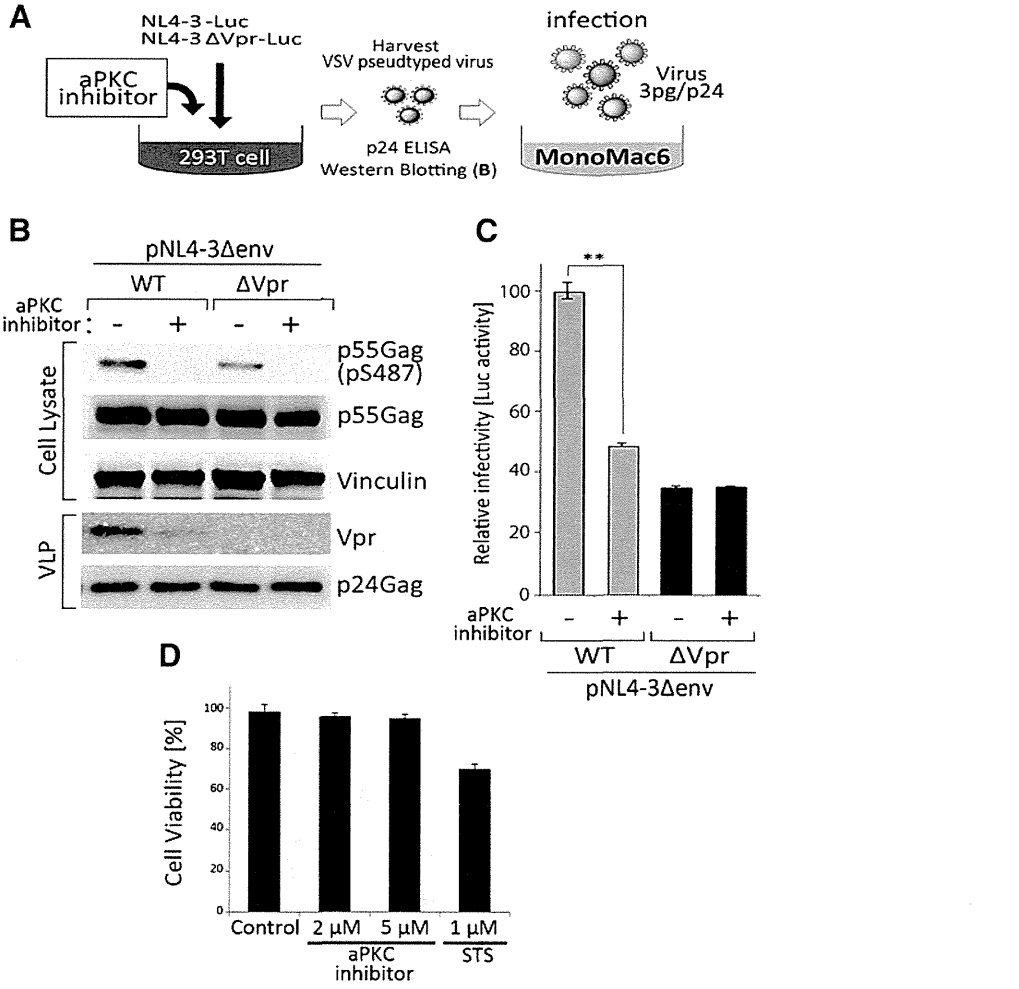



**Figure 6 The inhibition of aPKC significantly decreases single-round HIV-1 infection. (A)** Schematic representation of the experimental system. Briefly, 293T cells were either mock treated, or treated with aPKC inhibitor. After 4 hours, these cells were co-transfected with pNL4-3Δenv-luc or pNL4-3ΔenvΔVpr-luc and with pVSV-G. Viral release was measured through the quantification of p24CA antigen concentration in the culture supernatants at 48 hours post-transfection. MonoMac6 cells were infected with VSV-G pseudotyped WT and ΔVpr viruses for 48 hours. **(B)** The VSV-G pseudotyped WT and ΔVpr stocks generated from pNL4-3Δenv-luc and pNL4-3ΔenvΔVpr-luc with/without aPKC inhibitor treatment were analyzed by immunoblotting for the incorporation of Vpr into virion particles. **(C)** Viral infectivity was detected by measuring the luciferase activity in the cell lysates. Data are mean ± s.e.m. of three independent experiments. **(D)** Effects of aPKC inhibitors on viability of MonoMac6 cells. MonoMac6 cells were treated with aPKC inhibitor (2 or 5 μM) or 1 μM Staurosporine (STS) and analyzed for cell viability using trypan blue exclusion at 72 hours. Data are mean ± s.e.m. of three independent experiments: **$p < 0.01$, Student's t-test.

and a phenylalanine substitution at Ser487 (ΔPTAP/S487F) shows aberrant core formation and reduced viral infectivity in TZM-b1 cells [33]. More recently, steady state affinity analysis using a surface plasmon resonance sensorgram has revealed that the phosphorylated form of p6 at Ser487 has a stable binding affinity for cytoplasmic membranes [38]. These reports have therefore revealed that Gag Ser487 is a highly conserved phosphorylation site of likely crucial importance for HIV-1 infection. On the other hand, Radestock et al. recently reported in tissue culture experiments that the phosphorylation of Gag-p6 including Ser487 is dispensable for HIV-1 infectivity. These authors showed that asparagine substitutions at five serine residues (Ser487, Ser490, Ser494, Ser497 and Ser498) within the C-terminus of Gag p6 produced no impairment of Gag assembly or virus release and caused only very subtle deficiencies in viral infectivity in T-cell lines and in primary lymphocytes [39]. These discrepancies may be due to different experimental approaches using different Gag substitution mutants as well as different cell types. In contrast, our present approach is distinct from these earlier studies as we initially attempted to identify the kinases responsible for Gag-p6 phosphorylation and then explore their role in HIV-1 replication. Our current results clearly demonstrate that aPKC phosphorylates Gag-p6 and regulates the interaction of Gag with Vpr for

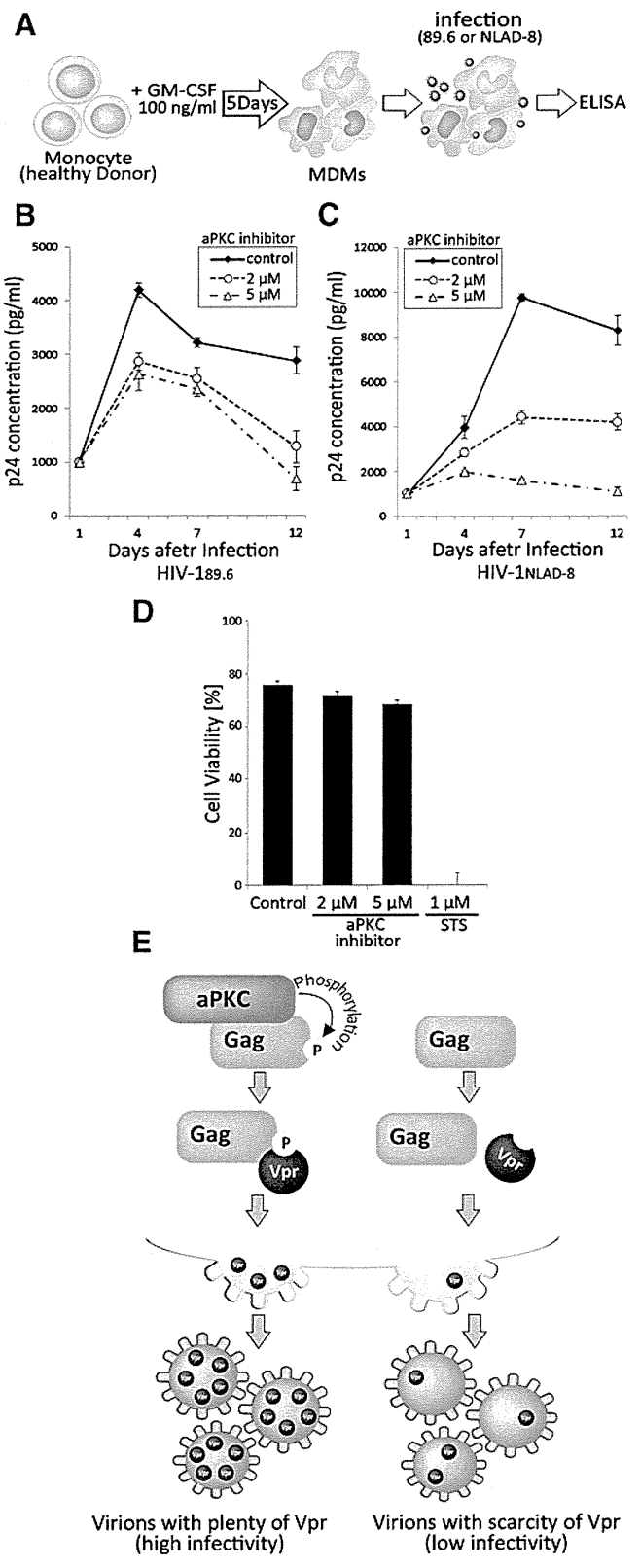



**Figure 7** (See legend on next page.)

(See figure on previous page.)
**Figure 7 The inhibition of aPKC significantly reduces replication competent HIV-1 infection. (A)** Schema of the experimental system using HIV-1 replication competent HIV-$1_{89.6}$ and HIV-$1_{NLAD-8}$. Monocytes were isolated from buffy coat from healthy blood donors by positive selection on Monocyte Enrichment Cocktail and density gradient centrifugation as described in Methods. MDMs were generated by culturing monocytes with 100 ng/ml granulocyte-macrophage colony-stimulation factor for 5 days before HIV-1 infection. MDMs were infected with 5 ng of p24 from **(B)** HIV-$1_{89.6}$ or **(C)** HIV-$1_{NLAD-8}$ virus and the levels of p24 capsid released into media during viral replication were assayed over a period of 12 days post infection. Data are the mean ± s.e.m. of three independent experiments: $^{**}P < 0.01$, Student's t-test. **(D)** Effects of aPKC inhibitor on viability of MDMs. MDMs cells were treated with aPKC inhibitor (2 or 5 μM) or 1 μM Staurosporine (STS) and analysed for cell viability using trypan blue exclusion at 96 hours. **(E)** Schematic model of our current study. aPKC phosphorylate HIV-1 Gag at Ser487. This phosphorylation promotes the interaction between Gag and Vpr, thereby facilitating viral infectivity in macrophages.

the incorporation of Vpr into virus particles. These specific effects of aPKC-mediated Gag-p6 phosphorylation are consistent with the evidence that the substitution of Gag Ser487 for Ala significantly decreases Vpr incorporation and viral infectivity. On the other hand, inhibition of aPKC in cells may have other additional effects on HIV-1 replication cycle rather than Gag phosphorylation for the Vpr incorporation. To observe the specific effect of aPKC on Gag phosphorylation, we created Gag and Vpr mutants devoid of the effect of aPKC and these mutants were less competent in virus replication. However, aPKC may regulate other cellular function directing HIV replication. Although our current data clearly demonstrate a crucial role of aPKC in Gag Ser487 phosphorylation and interaction Gag-Vpr to Vpr incorporation, further detailed analyses may be necessary to clarify the molecular signature of Gag p6 phosphorylation on multiple stages of the HIV-1 replication cycle.

We show from our current experiments that Gag Ser487 phosphorylation has a significant impact on p6-Vpr binding. Vpr is a non-structural viral protein that is incorporated into virions and possesses several characteristic features and functions that are known to play important roles in HIV-1 replication and disease progression [40]. The presence of a functional Vpr in viral particles is necessary for the efficient translocation of the pre-integration complex (PIC) into the nucleus and subsequent infection of primary monocytes/macrophages and other non-dividing cells [5,6]. Vpr also has a crucial role in viral replication, apoptosis, cell cycle arrest and in the down-regulation of immune activation [37,41-43]. Many Vpr functions are carried out by virion-associated Vpr [44], suggesting that the incorporation of Vpr into virus particles is an important event not only in HIV-1 replication but also in HIV-1 mediated cytopathogenesis.

Several previous reports have indicated that p6 is phosphorylated during HIV-1 infection [2,22]. However, these studies did not undertake any detailed investigation of the biological significance of this phosphorylation event through biochemical or structural analyses. Our current computer-assisted structural modeling and AlphaScreen homogenous proximity assays have revealed that the phosphorylated Gag at Ser487 binds more stably to Vpr whereas there was no significant difference in the interaction of Gag-p6 with Alix, consistent with previous reports [31,32]. The phosphorylation of Ser487 can create another hydrogen bond between Gag-Ser487 and Vpr-Gln44. In consistent with this data a previous study indicated that the site specific deletion of Gln44 resulted in the significant reduction of Vpr incorporation into virions [34]. We also demonstrate that Gag phosphorylation at Ser487 affects Vpr incorporation and this process could be mediated by Gln44 residue of Vpr.

We show in our current study that Gag phosphorylation on Ser487 itself does not affect the binding affinity of Gag with Alix. However, resultant Vpr interaction to Gag may hinder the Alix-Gag interaction at the LYPXnL motif. This may eliminate Alix from nascent VLP and impeded its ability to function in HIV-1 release in PTAP-deficient strains of HIV. On the other hands, Alix also interacts with the nucleocapsid (NC) domain of HIV-1 Gag in addition to binding the LYPXnL motif [45], there by linking Gag to components of ESCRT-III. Therefore, further analysis is needed to fully understand the molecular link between Gag phosphorylation and virus release through the Alix/LYPXnL pathway.

We further explored the physiological significance of Vpr incorporation into virions. Our current results clearly demonstrate that the inhibition of aPKC-mediated Vpr incorporation prominently reduces the viral infectivity in MDMs. These results together indicate that Gag phosphorylation by aPKC plays a crucial role in the HIV-1 infection of macrophages.

aPKC has been demonstrated to be involved in cell polarity and migration in a number of study models [46]. During cell migration, aPKC localizes on the leading edge of the plasma membrane where HIV-1 Gag is also localized in infected cells. It has been reported in an earlier study that aPKC is located at an immunological synapse with potential importance in cell-to-cell viral transfer [47]. It is thus plausible that aPKC may regulate the incorporation of Vpr into virions at the leading edges or the HIV-1 virological synapse in polarized cells [48]. It would be interesting to investigate whether aPKC cooperates with other factors in polarized HIV-1-infected cells in an additional mechanism to its function in Gag phosphorylation.

In the earlier study by Folgueira et al. [49], it was demonstrated that aPKC mediates the NF-κB transcriptional activation required for HIV-1 infection in U937 cells. It is of particular interest that aPKC is a one of the key regulators of HIV-1 infection. Our present findings also provide evidence for the involvement of aPKC in HIV-1 replication by showing that it directly phosphorylates Gag on Ser487, and that this phosphorylation mediates Vpr incorporation into virions. The targeting of aPKC activity is therefore a potential option as a novel therapeutic intervention against HIV-1 infection in combination with existing anti-retroviral treatments.

## Conclusions

We have identified aPKC as a host protein kinase that phosphorylates HIV-1 Gag at its Ser487 residue. Computer assisted structural modeling and subsequent biochemical assays revealed that the phosphorylation of Gag Ser487 enhances the association of Gag with Vpr and promotes the resultant incorporation of Vpr into virions. These events facilitate viral infectivity in macrophages. Hence, aPKC inhibition is a potential new therapeutic approach against HIV-1 infection in human macrophages.

## Methods

### Viral DNA constructs and plasmids

The HIV-1 reporter virus vectors pNL4-3ΔEnv-Luc and pNL4-3ΔEnvΔVpr-Luc were provided by Akifumi Takaori-Kondo (Kyoto University, Kyoto, Japan) [50,51]. The HIV-1 recombinant molecular clone pHIV-$1_{89.6}$ and pHIV-$1_{NLAD8}$ were provided by Akio Adachi (Tokushima University, Tokushima, Japan). The HIV-1 Gag and HIV-1 p6 (pNL4-3) derived-DNA fragment was generated by PCR and inserted into the pEU-E01-GST-MCS vector (Cellfree Sciences, Yokohama, Japan). Using this subcloned plasmid, we generated substitution mutants with PrimSTAR Max (Takara Bio Inc, Shiga, Japan) and the following primers for Ser487A,

5'-TTAACTGCGCTCAGATCACTCTTTGGC-3' and 5'-TCTGAGCGCAGTTAAAGGATACAGTTC-3'. Plasmids expressing HIV-1 Gag-Pol were provided by Jun Komano [52] (National Institute of Infectious Diseases, Tokyo, Japan). Expression vectors encoding aPKCλ wt and aPKCλ kn, a kinase-deficient mutant, have been previously described [53]. C-terminal Flag-tagged p55Gag (codon-optimized) has been previously described [54]. All the DNA experiments were approved by Gene and Recombination Experiment Safety Committee at the Yokohama City University School of Medicine.

### Antibodies and other reagents

The anti-p24 (CA) mouse monoclonal antibody (clone Kal-1) was purchased from Dako (Glostrup, Denmark). Anti-Flag (M2) and anti-Vinculin mouse monoclonal antibodies were obtained from Sigma (St. Louis, MO). Anti-PKCι mouse monoclonal antibody was from BD transduction (Franklin Lakes, NJ). Polyclonal rabbit anti-Vpr antibody was obtained from the AIDS research and Reference Reagent Program, National Institute of Allergy and Infectious Diseases (US National Institute of Health, Germantown, MD). The peptide specific antibody against PLT (pS) LRSLFGND (phosphorylated at Ser487 of Gag peptide from 484 to 495) was generated by Scrum Inc (Tokyo, Japan). The myristoylated (myr) PKC ζ peptide inhibitor myr-PKCζ (N-myr-Ser-Ile-Tyr-Arg-Arg-Gly-Ala-Arg-Arg-Trp-Arg-Lys-Leu-OH) and myr-PKC α and β (N-myr-Phe-Ala-Arg-Lys-Gly-Ala-Leu-Arg-Gln-$NH_2$) were purchased from Merck (Darmstadt, Germany). Akt inhibitor was obtained from Calbiochem (Darmstadt, Germany), and the PI3K inhibitor Wortmannin was obtained from Merck. The Cdk inhibitor roscovitine was purchased from Promega (Madison, WI). All inhibitors were dissolved in DMSO and stocks were aliquoted and stored at −60°C until use. The final concentration of each inhibitor used is indicated in the figure legends.

### Cells and viruses

Monocytes were isolated from buffy coat from healthy blood donors by positive selection on Monocyte Enrichment Cocktail (Stemcell, Tukwila, WA) and Lymphoprep (Stemcell) density gradient centrifugation with SepMate-50 (Stemcell). MDMs were generated by culturing monocytes with 100 ng/ml granulocyte-macrophage colony-stimulation factor for 5 days. 293T and HeLa cells were cultured in DMEM (Gibco-BRL, Rockville, MD) supplemented with 10% (V/V) fetal bovine serum (FBS) (Gibco-BRL). HIV-$1_{89.6}$ and HIV-$1_{NLAD-8}$ strains were produced in 293T cells. Vesicular stomatitis virus G glycoprotein (VSV-G)-pseudotyped viruses were produced in 293T cells cotransfected with reporter virus plasmid and VSV-G using the calcium-phosphate method. The culture supernatants were collected and subjected to quantification of HIV-1 particle yields by p24CA antigen capture enzyme-linked immunosorbent assay (ELISA) (Zepto Metrix, Buffalo, NY). Monocyte isolation and treatment were approved by the Ethics Committee at the Yokohama City University School of Medicine.

### *In vitro* protein production

A total of 287 cDNAs encoding human protein kinases were constructed as described previously [23]. The protein production method has also been described previously [55-57]. Briefly, DNA templates containing a biotin-ligating sequence were amplified by split-PCR using cDNAs and corresponding primers, and then used with the GenDecoder protein production system (Cell Free Science, Ehime, Japan). For HIV-1 Gag protein synthesis, *Gag* genes derived from the pNL4-3 proviral plasmid [58] were

generated by split-PCR, and used as template with a Wheat Germ Expression kit (Cell Free Science) in accordance with the manufacturer's instructions.

### Alphascreen-based protein-protein interaction assays

AlphaScreen assays were performed as described previously [23]. All recombinant proteins used here was synthesized using a wheat germ based cell-free system as described above. For each protein kinase, 1 μl of crude recombinant biotinylated construct from the human kinase library was incubated with 1 μl of crude GST-Gag or GST-DHFR in 10 μl of kinase assay buffer (100 mM Tris–HCl pH8.0, 10 mM $MgCl_2$, 0.1% Tween20, 0.1% BSA) at 37°C for 1 h in one well of a 384-well Optiplate (Perkin Elmer, Foster City, CA. In accordance with the AlphaScreen IgG (protein A) detection kit (Perkin Elmer) instruction manual, 15 μl of detection mixture containing 100 mM Tris–HCl pH 8.0, 0.01% Tween-20, 1 mg/ml BSA, 5 μg/ml Anti-FLAG antibody (GE healthcare, Buckinghamshire, UK), 5 ng streptavidin-coated donor beads and 5 ng anti-IgG (protein A) acceptor beads were added to each well followed by incubation at 26°C for 1 h. AlphaScreen signals from the mixture were detected using an EnVision device (PerkinElmer) with the AlphaScreen signal detection program.

### *In vitro* kinase assays

Biotinylated GST-Gag proteins were synthesized in wheat germ cell-free extracts as described above. The synthesized GST-Gag proteins were then purified using streptavidin conjugated magnet beads (Promega). The purified proteins on the beads were then incubated with recombinant aPKCiota (Cell Signaling Technology) in a 50 μl reaction mixture containing 20 mM Tris–HCl pH 7.5, 1 mM EDTA, 1 mM dithiothreitol, 150 mM NaCl, 5 mM $MgCl_2$, 0.05% Tween-20, 100 μM ATP and 2 μCi [$\gamma$-$^{32}$P] ATP. The reaction mixture was then incubated for 1 h at 37°C, and the products were subjected to electrophoresis on 10% SDS polyacrylamide gels and were detected with an image guider (BAS2500; Fujifilm, Tokyo, Japan).

### Western blotting

Cells were harvested at the indicated post-treatment time points with doxycycline, washed with phosphate-buffer saline (PBS), and treated with lysis buffer (0.02% sodium dodecyl sulfate [SDS], 0.5% Triton X-100, 300 mM NaCl, 20 mM Tris–HCl [pH 7.6], 1 mM EDTA, 1 mM dithiothreitol) for 20 min on ice. Multiple protease inhibitors, 200 μM sodium vanadate and 20 mM sodium fluoride were then added to the buffer. The samples were centrifuged at 18,000 g for 10 min at 4°C, and clarified cell extracts were assayed for protein concentration using a Bio-Rad kit. Equal amounts of proteins (20 ~ 50 μg) were resolved by SDS-10% polyacrylamide (acrylamide, 29.2; bisacrylamide, 0.8) gel electrophoresis (SDS-PAGE) in running buffer (250 mM glycine, 25 mM Tris, 0.1% SDS). The separated proteins were transferred to polyvinylidene difluoride membrane. The membranes were washed with blotting buffer (TBS containing 0.1% Tween 20) and blocked in 10% low-fat powdered milk in blotting buffer for 1 h at room temperature. Primary antibodies were added at appropriate dilutions in 3% bovine serum albumin in blotting buffer and rocked overnight at 4°C. The membranes were then further washed in blotting buffer and incubated with a horseradish peroxidase-conjugated secondary antibody at room temperature for 1 h. Target proteins were detected with an enhanced chemiluminescence detection system (GE Healthcare). Images were processed using Fluor Chem FC2 (Alpha Innotech Corp. Tokyo, Japan) with a cooled charge-coupled device (CCD) camera and assembled using Adobe Photoshop CS5 Extended.

### Identification of phosphorylation sites on HIV-1 gag by mass spectrometry

Samples were separated by SDS-PAGE (12.5%) and the gel was stained with Coomassie brilliant blue (CBB). Gag was excised from the stained gel and digested with trypsin in 50 mM $NH_4HCO_3$ (pH 8.0) for 12 h at 37°C. Phosphopeptides were enriched using Titansphere® Phos-TiO Kit (GLsciences, Tokyo, Japan), in accordance with the manufacturer's instructions. The enriched phosphopeptides were then analyzed by MALDI-TOF/TOF-MS (4800 proteomics analyzer, AB SCIEX, Foster City, CA). The resulting raw MS spectrum was processed using the 4000 Series Explorer Software (AB SCIEX, Framingham, MA) to generate Mascot generic format. The obtained MS and MS/MS data were then searched against the SwissProt database (January, 2013; 538849 sequences) using Mascot version 2.4.1 software (Matrix Science, London, UK), to identify proteins and protein modification. The search parameters were as follows: trypsin digestion with two missed cleavages permitted, variable modifications (oxidation of Met and phosphorylation of Ser, Thr, and Tyr), peptide mass tolerance for MS data ±0.15 Da, and fragment mass tolerance ±0.3 Da. Phosphopeptides were determined primarily using the Mascot program and were confirmed manually through raw MS/MS sequence data checking for the neutral loss of the phosphate group (−98).

### Analysis of structural data and structural model construction

The 3D structure of Alix with wild-type Gag-p6 was predicted by homology modeling using Molecular Operating Environment (MOE) (Chemical Computing Group, Canada). X-ray crystal structure of Gag-p6-Alix (Protein Data Bank [PDB] code: 2R02) was used as

template structure. Energy calculation was achieved with AMBER ff99 force field and the GB/VI implicit solvent energy function [59]. Next, on the basis of the predicted structural model of Alix with wild-type Gag-p6, 3D structures of Alix with Gag-p6S487A and phosphorylated Gag-p6-Ser487 were constructed using Molecular Builder in MOE.

3D structures of Vpr with wild-type Gag-p6, Gag-p6Ser487A, and phosphorylated Gag-p6-Ser487 were also predicted by docking simulations with ASEdock module in MOE, because of no complex structure of Gag-p6-Vpr. The complex structure was estimated with a nuclear magnetic resonance (NMR) structure of Vpr (PDB code: 1M8L [60]) and a NMR structure around helix II domain of Gag-p6 (Gag Y483 to S494) (PDB code: 2C55). Substitution and phosphorylation at Gag S487 were achieved with the Molecular Builder. Energy calculations in the docking simulations were achieved with the same force field as that for Gag-p6-Alix.

Finally, all of the constructed complex structures were thermodynamically optimized with energy minimization, to remove unfavorable steric contacts.

### *Bimolecular fluorescence complementation assay (BiFC)*

To detect interaction of Gag with Vpr, we used the BiFC technique. Briefly, two fragments of Kusabira-Green (KG) fluorescent protein are brought together by the interaction of two proteins fused to these fragments, thus allowing specific detection of interaction in living cells (Amalgaam). Vpr or Vpr Q44E were cloned into phmKGN-MN and Gag or GagSer487A into phmKGC-MC. 293T cells were cotransfected with 0.7 μg of the Vpr construct and 0.5 μg of the Gag construct. Two days post transfection, cells were harvested and then subjected to the flow cytometry for measuring BiFC signal as reported previously [34].

### Immunoprecipitation

Cells were lysed in Lysis buffer containing 50 mM Tris–HCl (pH 8.0), 150 mM NaCl, 1 mM EDTA, 1 mM DTT with Complete protease inhibitor cocktail (Roche Molecular Biochemicals, Indianapolis, IN) and PhosSTOP phosphatase inhibitor cocktail (Roche Molecular Biochemicals). Lysate were cleared by centrifugation at 12,000 × g for 15 min, followed by pull down using with anti-Flag M2 affinity Gel (Sigma). Samples were separated by SDS-PAGE and analysed by Western blot analyses.

### Single-cycle virus release assays

For infection-based assays, cells were infected with VSV-G-pseudotyped HIV-1 at an moi (multiplicity of infection) of 0.01 or 0.2 for eight hours and cultured for two days. In experiments using kinase inhibitors, cells were treated with each inhibitor at 12 h before virus infection. Virus-containing supernatants were harvested and filtered to remove cell debris, and viral p24 antigens were measured using an ELISA kit (Zepto Metrix). The cell lysates were prepared using HBST buffer (10 mM HEPES, pH 7.4, 150 mM NaCl, 0.5% Triton X-100) containing a protease inhibitor cocktail (Roche). Immunoblotting assays and the antibodies used have been described previously [61]. The culture supernatants and cell lysates were subjected to p24 ELISA or immunoblotting assays, as described above.

### HIV-1 production assay

Primary human macrophages were infected with HIV-$1_{89.6}$ or HIV-$1_{NLAD-8}$ virus. Two days post-infection, these cells were washed with PBS to eliminate the presence of virus. After washing, the cells were cultured either in media alone or media containing aPKC inhibitor. Infected macrophages were cultured for 12 days, during which time viral supernatants were collected and fresh media with inhibitors was also added every three days. The p24 levels contained in each viral supernatant sample was monitored using p24 ELISA (Zepto Metrix) in accordance with the manufacturer's protocol.

#### Competing interests

The authors declare that they have no competing interests.

#### Authors' contributions

AK, ST, HO, KM, AO and AI performed experiments. AK, ST, TS, SM, HK, WS, HS, HH, SO, NY and AR participated in the design of the study, the analysis of the data. AK and AR wrote the manuscript. All authors read and approved the final manuscript.

#### Acknowledgements

We gratefully acknowledge Akifumi Takaori-Kondo (Kyoto University) for providing the reporter virus vectors pNL4-3ΔEnv-Luc and pNL4-3ΔEnvΔVpr-Luc, Akio Adachi (Tokushima University) for providing Flag-Vpr expression vector, HIV-1 molecular clone vectors for HIV-$1_{89.6}$, and HIV-$1_{NLAD-8}$, Akinori Takaoka (Hokkaido University) for kindly providing a material and discussion, Andrés Finzi (Université de Montréal) for helpful discussion, Noriko Ikawa (Yokohama City University) for technical assistance. HIV-1 Vpr (1–50) antiserum was obtained through the AIDS Research and Reference Reagent Program, Division of AIDS, NIAID, NIH from Jeffrey Kopp.

#### Author details

[1]Department of Microbiology, Yokohama City University School of Medicine, Yokohama, Kanagawa, Japan. [2]Venture Business Laboratory, Ehime University, Matsuyama, Ehime, Japan. [3]Proteo-Science Center, Ehime University, Matsuyama, Ehime, Japan. [4]Clinical Research Center, National Hospital Organization Nagoya Medical Center, Nagoya, Aichi, Japan. [5]Pathogen Genomics Center, National Institute of Infectious Diseases, Musashi Murayama, Tokyo, Japan. [6]Supramolecular Biology, International Graduate School of Arts and Sciences, Yokohama City University, Yokohama, Kanagawa, Japan. [7]Infectious Disease Surveillance Center, National Institute of Infectious Diseases, Musashi Murayama, Tokyo, Japan. [8]Department of Molecular Biology, Yokohama City University School of Medicine, Yokohama, Kanagawa, Japan. [9]Department of Microbiology, National University of Singapore, Singapore, Singapore.

Received: 25 July 2013 Accepted: 12 January 2014
Published: 22 January 2014

## References


1. Barnitz RA, Wan F, Tripuraneni V, Bolton DL, Lenardo MJ: **Protein kinase A phosphorylation activates Vpr-induced cell cycle arrest during human immunodeficiency virus type 1 infection.** *J Virol* 2010, **84**(13):6410–6424.
2. Hemonnot B, Cartier C, Gay B, Rebuffat S, Bardy M, Devaux C, Boyer V, Briant L: **The host cell MAP kinase ERK-2 regulates viral assembly and release by phosphorylating the p6gag protein of HIV-1.** *J Biol Chem* 2004, **279**(31):32426–32434.
3. Ammosova T, Berro R, Jerebtsova M, Jackson A, Charles S, Klase Z, Southerland W, Gordeuk VR, Kashanchi F, Nekhai S: **Phosphorylation of HIV-1 Tat by CDK2 in HIV-1 transcription.** *Retrovirology* 2006, **3**:78.
4. Adamson CS, Freed EO: **Human immunodeficiency virus type 1 assembly, release, and maturation.** *Adv Pharmacol* 2007, **55**:347–387.
5. Subbramanian RA, Kessous-Elbaz A, Lodge R, Forget J, Yao XJ, Bergeron D, Cohen EA: **Human immunodeficiency virus type 1 Vpr is a positive regulator of viral transcription and infectivity in primary human macrophages.** *J Exp Med* 1998, **187**(7):1103–1111.
6. Connor RI, Chen BK, Choe S, Landau NR: **Vpr is required for efficient replication of human immunodeficiency virus type-1 in mononuclear phagocytes.** *Virology* 1995, **206**(2):935–944.
7. Levy DN, Refaeli Y, Weiner DB: **Extracellular Vpr protein increases cellular permissiveness to human immunodeficiency virus replication and reactivates virus from latency.** *J Virol* 1995, **69**(2):1243–1252.
8. de Marco A, Muller B, Glass B, Riches JD, Krausslich HG, Briggs JA: **Structural analysis of HIV-1 maturation using cryo-electron tomography.** *PLoS Pathog* 2010, **6**(11):e1001215.
9. Morita E, Sundquist WI: **Retrovirus budding.** *Annu Rev Cell Dev Biol* 2004, **20**:395–425.
10. Demirov DG, Orenstein JM, Freed EO: **The late domain of human immunodeficiency virus type 1 p6 promotes virus release in a cell type-dependent manner.** *J virology* 2002, **76**(1):105–117.
11. Garrus JE, von Schwedler UK, Pornillos OW, Morham SG, Zavitz KH, Wang HE, Wettstein DA, Stray KM, Cote M, Rich RL, *et al*: **Tsg101 and the vacuolar protein sorting pathway are essential for HIV-1 budding.** *Cell* 2001, **107**(1):55–65.
12. Strack B, Calistri A, Craig S, Popova E, Gottlinger HG: **AIP1/ALIX is a binding partner for HIV-1 p6 and EIAV p9 functioning in virus budding.** *Cell* 2003, **114**(6):689–699.
13. von Schwedler UK, Stuchell M, Muller B, Ward DM, Chung HY, Morita E, Wang HE, Davis T, He GP, Cimbora DM, *et al*: **The protein network of HIV budding.** *Cell* 2003, **114**(6):701–713.
14. Fujii K, Hurley JH, Freed EO: **Beyond Tsg101: the role of Alix in 'ESCRTing' HIV-1.** *Nat rev Microbiol* 2007, **5**(12):912–916.
15. Bieniasz PD: **Late budding domains and host proteins in enveloped virus release.** *Virology* 2006, **344**(1):55–63.
16. Morita E, Sandrin V, McCullough J, Katsuyama A, Baci Hamilton I, Sundquist WI: **ESCRT-III protein requirements for HIV-1 budding.** *Cell Host Microbe* 2011, **9**(3):235–242.
17. Fujii K, Munshi UM, Ablan SD, Demirov DG, Soheilian F, Nagashima K, Stephen AG, Fisher RJ, Freed EO: **Functional role of Alix in HIV-1 replication.** *Virology* 2009, **391**(2):284–292.
18. Salgado GF, Marquant R, Vogel A, Alves ID, Feller SE, Morellet N, Bouaziz S: **Structural studies of HIV-1 Gag p6ct and its interaction with Vpr determined by solution nuclear magnetic resonance.** *Biochemistry* 2009, **48**(11):2355–2367.
19. Paxton W, Connor RI, Landau NR: **Incorporation of Vpr into human immunodeficiency virus type 1 virions: requirement for the p6 region of gag and mutational analysis.** *J Virol* 1993, **67**(12):7229–7237.
20. Belzile JP, Abrahamyan LG, Gerard FC, Rougeau N, Cohen EA: **Formation of mobile chromatin-associated nuclear foci containing HIV-1 Vpr and VPRBP is critical for the induction of G2 cell cycle arrest.** *PLoS Pathog* 2010, **6**(9):e1001080.
21. Solbak SM, Reksten TR, Roder R, Wray V, Horvli O, Raae AJ, Henklein P, Fossen T: **HIV-1 p6-Another viral interaction partner to the host cellular protein cyclophilin A.** *Biochim Biophys Acta* 2012, **1824**(4):667–678.
22. Muller B, Patschinsky T, Krausslich HG: **The late-domain-containing protein p6 is the predominant phosphoprotein of human immunodeficiency virus type 1 particles.** *J Virol* 2002, **76**(3):1015–1024.
23. Tadokoro D, Takahama S, Shimizu K, Hayashi S, Endo Y, Sawasaki T: **Characterization of a caspase-3-substrate kinome using an N- and C-terminally tagged protein kinase library produced by a cell-free system.** *Cell Death Dis* 2010, **1**:e89.
24. Burnette B, Yu G, Felsted RL: **Phosphorylation of HIV-1 gag proteins by protein kinase C.** *J Biol Chem* 1993, **268**(12):8698–8703.
25. Cartier C, Sivard P, Tranchat C, Decimo D, Desgranges C, Boyer V: **Identification of three major phosphorylation sites within HIV-1 capsid. Role of phosphorylation during the early steps of infection.** *J Biol Chem* 1999, **274**(27):19434–19440.
26. Newton AC: **Regulation of protein kinase C.** *Curr Opin Cell Biol* 1997, **9**(2):161–167.
27. Guendel I, Agbottah ET, Kehn-Hall K, Kashanchi F: **Inhibition of human immunodeficiency virus type-1 by cdk inhibitors.** *AIDS Res Ther* 2010, **7**(1):7.
28. Deregibus MC, Cantaluppi V, Doublier S, Brizzi MF, Deambrosis I, Albini A, Camussi G: **HIV-1-Tat protein activates phosphatidylinositol 3-kinase/AKT-dependent survival pathways in Kaposi's sarcoma cells.** *J Biol Chem* 2002, **277**(28):25195–25202.
29. Chugh P, Fan S, Planelles V, Maggirwar SB, Dewhurst S, Kim B: **Infection of human immunodeficiency virus and intracellular viral Tat protein exert a pro-survival effect in a human microglial cell line.** *J Mol Biol* 2007, **366**(1):67–81.
30. Yu G, Shen FS, Sturch S, Aquino A, Glazer RI, Felsted RL: **Regulation of HIV-1 gag protein subcellular targeting by protein kinase C.** *J Biol Chem* 1995, **270**(9):4792–4796.
31. Fisher RD, Chung HY, Zhai Q, Robinson H, Sundquist WI, Hill CP: **Structural and biochemical studies of ALIX/AIP1 and its role in retrovirus budding.** *Cell* 2007, **128**(5):841–852.
32. Lazert C, Chazal N, Briant L, Gerlier D, Cortay JC: **Refined study of the interaction between HIV-1 p6 late domain and ALIX.** *Retrovirology* 2008, **5**:39.
33. Votteler J, Neumann L, Hahn S, Hahn F, Rauch P, Schmidt K, Studtrucker N, Solbak SM, Fossen T, Henklein P, *et al*: **Highly conserved serine residue 40 in HIV-1 p6 regulates capsid processing and virus core assembly.** *Retrovirology* 2011, **8**:11.
34. Venkatachari NJ, Walker LA, Tastan O, Le T, Dempsey TM, Li Y, Yanamala N, Srinivasan A, Klein-Seetharaman J, Montelaro RC, *et al*: **Human immunodeficiency virus type 1 Vpr: oligomerization is an essential feature for its incorporation into virus particles.** *Virology J* 2010, **7**:119.
35. Balliet JW, Kolson DL, Eiger G, Kim FM, McGann KA, Srinivasan A, Collman R: **Distinct effects in primary macrophages and lymphocytes of the human immunodeficiency virus type 1 accessory genes vpr, vpu, and nef: mutational analysis of a primary HIV-1 isolate.** *Virology* 1994, **200**(2):623–631.
36. Heinzinger NK, Bukinsky MI, Haggerty SA, Ragland AM, Kewalramani V, Lee MA, Gendelman HE, Ratner L, Stevenson M, Emerman M: **The Vpr protein of human immunodeficiency virus type 1 influences nuclear localization of viral nucleic acids in nondividing host cells.** *Proc Natl Acad Sci USA* 1994, **91**(15):7311–7315.
37. Vodicka MA, Koepp DM, Silver PA, Emerman M: **HIV-1 Vpr interacts with the nuclear transport pathway to promote macrophage infection.** *Genes Dev* 1998, **12**(2):175–185.
38. Solbak SM, Reksten TR, Hahn F, Wray V, Henklein P, Halskau O, Schubert U, Fossen T: **HIV-1 p6 - a structured to flexible multifunctional membrane-interacting protein.** *Biochim Biophys Acta* 2013, **1828**(2):816–823.
39. Radestock B, Morales I, Rahman SA, Radau S, Glass B, Zahedi RP, Muller B, Krausslich HG: **Comprehensive mutational analysis reveals p6Gag phosphorylation to be dispensable for HIV-1 morphogenesis and replication.** *J Virol* 2013, **87**(2):724–734.
40. Lai M, Chen J: **The role of Vpr in HIV-1 disease progression is independent of its G2 arrest induction function.** *Cell Cycle* 2006, **5**(19):2275–2280.
41. Sawaya BE, Khalili K, Gordon J, Taube R, Amini S: **Cooperative interaction between HIV-1 regulatory proteins Tat and Vpr modulates transcription of the viral genome.** *J Biol Chem* 2000, **275**(45):35209–35214.
42. Chang F, Re F, Sebastian S, Sazer S, Luban J: **HIV-1 Vpr induces defects in mitosis, cytokinesis, nuclear structure, and centrosomes.** *Mol Biol Cell* 2004, **15**(4):1793–1801.
43. Ramanathan MP, Curley E 3rd, Su M, Chambers JA, Weiner DB: **Carboxyl terminus of hVIP/mov34 is critical for HIV-1-Vpr interaction and glucocorticoid-mediated signaling.** *J Biol Chem* 2002, **277**(49):47854–47860.
44. Romani B, Engelbrecht S: **Human immunodeficiency virus type 1 Vpr: functions and molecular interactions.** *J Gen Virol* 2009, **90**(Pt 8):1795–1805.

45. Dussupt V, Javid MP, Abou-Jaoude G, Jadwin JA, de La Cruz J, Nagashima K, Bouamr F: **The nucleocapsid region of HIV-1 Gag cooperates with the PTAP and LYPXnL late domains to recruit the cellular machinery necessary for viral budding.** *PLoS Pathog* 2009, **5**(3):e1000339.
46. Rosse C, Linch M, Kermorgant S, Cameron AJ, Boeckeler K, Parker PJ: **PKC and the control of localized signal dynamics.** *Nat Rev Mol Cell Biol* 2010, **11**(2):103–112.
47. Yuseff MI, Reversat A, Lankar D, Diaz J, Fanget I, Pierobon P, Randrian V, Larochette N, Vascotto F, Desdouets C, *et al*: **Polarized secretion of lysosomes at the B cell synapse couples antigen extraction to processing and presentation.** *Immunity* 2011, **35**(3):361–374.
48. Gousset K, Ablan SD, Coren LV, Ono A, Soheilian F, Nagashima K, Ott DE, Freed EO: **Real-time visualization of HIV-1 GAG trafficking in infected macrophages.** *PLoS Pathog* 2008, **4**(3):e1000015.
49. Folgueira L, McElhinny JA, Bren GD, MacMorran WS, Diaz-Meco MT, Moscat J, Paya CV: **Protein kinase C-zeta mediates NF-kappa B activation in human immunodeficiency virus-infected monocytes.** *J Virol* 1996, **70**(1):223–231.
50. Kobayashi M, Takaori-Kondo A, Miyauchi Y, Iwai K, Uchiyama T: **Ubiquitination of APOBEC3G by an HIV-1 Vif-Cullin5-Elongin B-Elongin C complex is essential for Vif function.** *J Biol Chem* 2005, **280**(19):18573–18578.
51. Izumi T, Io K, Matsui M, Shirakawa K, Shinohara M, Nagai Y, Kawahara M, Kobayashi M, Kondoh H, Misawa N, *et al*: **HIV-1 viral infectivity factor interacts with TP53 to induce G2 cell cycle arrest and positively regulate viral replication.** *Proc Natl Acad Sci USA* 2010, **107**(48):20798–20803.
52. Urano E, Aoki T, Futahashi Y, Murakami T, Morikawa Y, Yamamoto N, Komano J: **Substitution of the myristoylation signal of human immunodeficiency virus type 1 Pr55Gag with the phospholipase C-delta1 pleckstrin homology domain results in infectious pseudovirion production.** *J Gen Virol* 2008, **89**(Pt 12):3144–3149.
53. Yamanaka T, Horikoshi Y, Suzuki A, Sugiyama Y, Kitamura K, Maniwa R, Nagai Y, Yamashita A, Hirose T, Ishikawa H, *et al*: **PAR-6 regulates aPKC activity in a novel way and mediates cell-cell contact-induced formation of the epithelial junctional complex.** *Genes Cells* 2001, **6**(8):721–731.
54. Ryo A, Tsurutani N, Ohba K, Kimura R, Komano J, Nishi M, Soeda H, Hattori S, Perrem K, Yamamoto M, *et al*: **SOCS1 is an inducible host factor during HIV-1 infection and regulates the intracellular trafficking and stability of HIV-1 Gag.** *Proc Natl Acad Sci USA* 2008, **105**(1):294–299.
55. Sawasaki T, Ogasawara T, Morishita R, Endo Y: **A cell-free protein synthesis system for high-throughput proteomics.** *Proc Natl Acad Sci USA* 2002, **99**(23):14652–14657.
56. Sawasaki T, Morishita R, Gouda MD, Endo Y: **Methods for high-throughput materialization of genetic information based on wheat germ cell-free expression system.** *Methods Mol Biol* 2007, **375**:95–106.
57. Takai K, Sawasaki T, Endo Y: **Practical cell-free protein synthesis system using purified wheat embryos.** *Nat Protoc* 2010, **5**(2):227–238.
58. Adachi A, Gendelman HE, Koenig S, Folks T, Willey R, Rabson A, Martin MA: **Production of acquired immunodeficiency syndrome-associated retrovirus in human and nonhuman cells transfected with an infectious molecular clone.** *J Virol* 1986, **59**(2):284–291.
59. Labute P: **The generalized Born/volume integral implicit solvent model: estimation of the free energy of hydration using London dispersion instead of atomic surface area.** *J Comput Chem* 2008, **29**(10):1693–1698.
60. Morellet N, Bouaziz S, Petitjean P, Roques BP: **NMR structure of the HIV-1 regulatory protein VPR.** *J Mol Biol* 2003, **327**(1):215–227.
61. Miyakawa K, Ryo A, Murakami T, Ohba K, Yamaoka S, Fukuda M, Guatelli J, Yamamoto N: **BCA2/Rabring7 promotes tetherin-dependent HIV-1 restriction.** *PLoS Pathog* 2009, **5**(12):e1000700.

doi:10.1186/1742-4690-11-9
**Cite this article as:** Kudoh *et al.*: The phosphorylation of HIV-1 Gag by atypical protein kinase C facilitates viral infectivity by promoting Vpr incorporation into virions. *Retrovirology* 2014 **11**:9.

**Submit your next manuscript to BioMed Central and take full advantage of:**

- Convenient online submission
- Thorough peer review
- No space constraints or color figure charges
- Immediate publication on acceptance
- Inclusion in PubMed, CAS, Scopus and Google Scholar
- Research which is freely available for redistribution

Submit your manuscript at
www.biomedcentral.com/submit

BioMed Central

Author's personal copy

Biochimica et Biophysica Acta 1834 (2013) 601–610

Contents lists available at SciVerse ScienceDirect

Biochimica et Biophysica Acta

journal homepage: www.elsevier.com/locate/bbapap

# Proteomic identification of differentially expressed genes during differentiation of cynomolgus monkey (*Macaca fascicularis*) embryonic stem cells to astrocyte progenitor cells *in vitro*

Kuniko Akama [a,b,*], Tomoe Horikoshi [a], Takashi Nakayama [c], Masahiro Otsu [d,1], Noriaki Imaizumi [a], Megumi Nakamura [e], Tosifusa Toda [e,2], Michiko Inuma [f], Hisashi Hirano [g], Yasushi Kondo [h], Yutaka Suzuki [h], Nobuo Inoue [d]

[a] *Department of Chemistry, Graduate School of Science, Chiba University, Chiba 263–8522, Japan*
[b] *Center for General Education, Chiba University, Chiba 263–8522, Japan*
[c] *Department of Biochemistry, Yokohama City University School of Medicine, Yokohama 236–0004, Japan*
[d] *Laboratory of Regenerative Neurosciences, Graduate School of Human Health Science, Tokyo Metropolitan University, Tokyo 116–8551, Japan*
[e] *Proteome, Mechanism of Aging, Tokyo Metropolitan Institute of Gerontology, Tokyo 173–0015, Japan*
[f] *Advanced Medical Research Center, Yokohama City University, Yokohama 236–0004, Japan*
[g] *Department of Supramolecular Biology, Graduate School of Nanobioscience, Yokohama City University, Yokohama 230-0045, Japan*
[h] *Regenerative Medicine, Advanced Medical Research Laboratory, Mitsubishi Tanabe Pharma Co, Osaka 541–8505, Japan*

ARTICLE INFO

*Article history:*
Received 15 June 2012
Received in revised form 13 November 2012
Accepted 3 December 2012
Available online 8 December 2012

*Keywords:*
Embryonic stem cell
Neural stem cell
Astrocyte progenitor cell
Cellular retinoic acid binding protein 1
Collapsin response mediator protein 2

ABSTRACT

Understanding astrocytogenesis is valuable for the treatment of nervous system disorders, as astrocytes provide structural, metabolic and defense support to neurons, and regulate neurons actively. However, there is limited information about the molecular events associated with the differentiation from primate ES cells to astrocytes. We therefore investigated the differentially expressed proteins in early astrocytogenesis, from cynomolgus monkey ES cells (CMK6 cell line) into astrocyte progenitor (AstP) cells via the formation of primitive neural stem spheres (Day 4), mature neural stem spheres (NSS), and neural stem (NS) cells *in vitro*, using two-dimensional gel electrophoresis (2-DE) and liquid chromatography-tandem mass spectrometry (LC-MS-MS). We identified 66 differentially expressed proteins involved in these five differentiation stages. Together with the results of Western blotting, RT-PCR, and a search of metabolic pathways related to the identified proteins, these results indicated that collapsin response mediator protein 2 (CRMP2), its phosphorylated forms, and cellular retinoic acid binding protein 1 (CRABP1) were upregulated from ES cells to Day 4 and NSS cells, to which differentiation stages apoptosis-associated proteins such as caspases were possibly related; Phosphorylated CRMP2s were further upregulated but CRABP1 was downregulated from NSS cells to NS cells, during which differentiation stage considerable axon guidance proteins for development of growth cones, axon attraction, and repulsion were possibly readied; Nonphosphorylated CRMP2 was downregulated but CRABP1 was re-upregulated from NS cells to AstP cells, in which differentiation stage reorganization of actin cytoskeleton linked to focal adhesion was possibly accompanied. These results provide insight into the molecular basis of early astrocytogenesis in monkey.

© 2012 Elsevier B.V. All rights reserved.

## 1. Introduction

Astrocytes are important for providing structural, metabolic and defense support to neurons, and for regulating neurons actively: Astrocytes take up $K^+$ ion and glutamate, which are released from activated neurons, modulating excitability of neurons; Astrocytes release glutamine, the precursor of neurotransmitters glutamate and gamma-amino butyric acid, and release ATP, which regulate excitability of neurons positively [1–3]; Astrocytes release pyruvate and lactate to support neuronal metabolism; Glutathione and ascorbate, which are released from astrocytes, work as antioxidants [2]. In addition, astrocytes promote neuronal differentiation of adult NS cells through ephrin-B signaling [4]. Astrocytes form the brain–blood barrier, and maintain water

*Abbreviations:* ACM, astrocyte-conditioned medium; AstP, astrocyte progenitor; CRABP1, cellular retinoic acid binding protein 1; CRMP2, collapsin response mediator protein 2; Day 4, primitive neural stem spheres; 2-DE, two-dimensional gel electrophoresis; EGF, epidermal growth factor; ES, embryonic stem; FABP7, fatty acid binding protein 7; FGF, fibroblast growth factor; GFAP, glial fibrillary acidic protein; IEF, isoelectric focusing; IPG, immobilized pH gradient; LC-MS-MS, liquid chromatography-tandem mass spectrometry; MS, mass spectrometry; NS, neural stem; NSS, neural stem spheres; PMF, peptide mass fingerprinting; T-TBS, TBS containing 0.05% Tween.

* Corresponding author at: Center for General Education and Department of Chemistry, Graduate School of Science, Chiba University, Yayoi-Cho 1-33, Inage-Ku, Chiba, Chiba 263-8522, Japan. Tel.: +81 43 290 2795; fax: +81 43 290 2874.
*E-mail address:* akama@faculty.chiba-u.jp (K. Akama).
[1] Present address: Department of Chemistry, Kyorin University, School of Medicine, Tokyo 181-8611, Japan.
[2] Present address: Advanced Medical Research Center, Yokohama City University, Yokohama 236-0004, Japan.

1570-9639/$ – see front matter © 2012 Elsevier B.V. All rights reserved.
http://dx.doi.org/10.1016/j.bbapap.2012.12.002

Author's personal copy



and ion homeostasis in the brain together with endothelial cells [1]. Moreover, astrocytes have been shown to act as NS cells [5]. Although NS cells were thought to exhibit an undifferentiated phenotype, they have been shown to be committed to the astrocytic lineage from radial glia in embryos to a subpopulation of astrocytes in adults [6]. Thus, the astrocytic lineage arising from neuroepithelial cells constitutes an expanded population with diverse functions and morphologies. Mi and Barres [7] provide data suggesting the presence of astrocyte precursor cells without glial fibrillary acidic protein (GFAP) immunoreactivity from the developing rat optic nerve, of which cells begin to express GFAP upon differentiation induced by ciliary neurotrophic factor or by leukemia inhibitory factor (LIF). Seidman et al. [8] describe astrocyte restricted precursor cells present in E16 mouse cerebellum that do not express GFAP, of which cells begin to express GFAP upon differentiation induced by fibroblast growth factor-2 (FGF-2).

Nakayama and co-workers have established a unique method for efficiently producing NS cells with high purity from mouse, monkey, and human embryonic stem cells *via* the formation of neural stem spheres (NSS) under free-floating conditions in astrocyte-conditioned medium (ACM) *in vitro* [9–15]. Under this method designated as NSS method, neurogenesis has been shown to be very similar to that of early neurogenesis *in vivo* [13]. Many Nestin-positive NS cells migrate from NSS by culturing NSS in Neurobasal medium supplemented with B-27, FGF-2, and EGF on an adhesive substrate. The migrated monkey NS cells expressed Nestin (99.5%±0.5%) [14]. Furthermore, the NS cells can be differentiated almost exclusively into GFAP-positive astrocytes by withdrawing FGF-2 fibroblast growth factor-2 (FGF-2) and/or epidermal growth factor (EGF) from the medium without any additional instructions [11,12,15]. However, there is currently limited information about the molecular events associated with the transition from primate ES cells to astrocytes, and the mechanisms underlying the differentiation have not been elucidated fully.

The monkey is considered a promising animal model in regenerative medicine, as the monkey shares many physiological similarities with humans and has several advantages with regard to breeding and handling. Since monkey ES cells differentiate into neural cells about twice more slowly than mouse ES cells [9,10,12–14], it is thought that we can study the global developmental processes in detail from monkey ES cells to NS cells via NSS cells and from NS cells to AstP cells, whereas it is difficult to investigate these processes in mouse. In this study, we investigated the differentially expressed proteins in early astrocytogenesis in monkey, from ES cells into AstP cells via NSS cells and NS cells, using a 2-DE-based proteomic approach, and searched metabolic pathways related to the differentially regulated proteins. The results provided insight into the molecular events associated with the transition from ES cells to AstP cells.

## 2. Materials and methods

### 2.1. Cell culture

The CMK6 ES cell line of cynomolgus monkey (*Macaca fascicularis*) [16] was maintained on a feeder layer of mitotically inactivated mouse embryonic fibroblasts in DMEM (Invitrogen, Carlsbad, CA) supplemented with 1000 U/ml leukemia inhibitory factor (Chemicon, Temecula, CA), 1 mM 2-mercaptoethanol (Invitrogen), and 15% knockout serum replacement (Invitrogen). Colonies of ES cells were collected by picking with glass capillaries. To give rise to NSS, colonies of undifferentiated ES cells were picked up and cultured under free-floating conditions in ACM supplemented with 20 ng/mL of recombinant human FGF-2 (R&D Systems, Minneapolis, MN) and 20 ng/mL of recombinant human EGF (R&D Systems), as reported previously [9–15]. The primitive and mature NSS cultured for 4 days and for 12 days under the conditions described above were collected as Day 4 cells and NSS cells, respectively, by centrifugation at 700×*g* for 5 min. The NSS were plated onto Matrigel-coated dishes and encouraged to proliferate by culturing in Neurobasal medium (Gibco Invitrogen Corp. Grand Island, NY) supplemented with 2% B-27 (Gibco Invitrogen Corp.), 20 ng/mL FGF-2, and 20 ng/mL of EGF. From the adherent NSS, the NS cells migrated to the surrounding areas. After removal of the NSS by picking up with glass capillaries, the migrated NS cells were collected using a cell scraper followed by centrifugation. Differentiation of NS cells to AstP cells was initiated by withdrawal of FGF-2 and EGF, and continued for 7 days as reported previously [11]. The whole protocol of the differentiation from monkey ES cells to AstP cells is shown in Supplementary Fig. 1.

### 2.2. Immunofluorescence analysis

The cells were fixed in 4% paraformaldehyde in phosphate-buffered saline (PBS). Immunocytochemistry was performed using standard protocols [9–11] and antibody against GFAP (Chemicon International Inc., Temecula, California). Alexa Fluor 594-labeled secondary antibody was purchased from Molecular Probes Inc. (Eugene, Oregon). Specimens were examined using a fluorescence microscope (Eclipse E800, Nikon, Tokyo, Japan) equipped with phase-contrast optics.

### 2.3. Sample preparation for 2-DE

The cells were washed twice by suspending in cold PBS followed by centrifugation, and stored as cell pellets at −80 °C. Aliquots of the cell pellets were suspended in lysis buffer containing 5 M urea, 2 M thiourea, 2% (w/v) CHAPS (Dojindo Laboratories, Kumamoto, Japan), 2% (w/v) sulfobetaine 10 (Amresco, Solon, OH), 2% Pharmalyte 3–10 (Amersham Biosciences Inc., Piscataway, NJ) with protease inhibitors (Pierce Chemicals, Rockford, IL), and phosphatase inhibitor cocktails 1 and 2 (Sigma-Aldrich, St. Louis, MO). The cell suspensions were sonicated using an ultrasonic vibrator (UR200P; Tomy, Tokyo, Japan). The sonicated cells were centrifuged at 12,000×*g* for 10 min, and the supernatants were ultracentrifuged at 100,000×*g* for 30 min to remove DNA. The extracted proteins were reduced and carbamidomethylated with a ReadyPrep Reduction-alkylation kit (Bio-Rad, Richmond, CA), and desalted with a 2-D Clean-Up kit (GE Healthcare Biosciences, Fairfield, CT). The protein content of each supernatant was measured with a 2-D Quant Kit (GE Healthcare Biosciences).

### 2.4. High-resolution 2-DE

Proteins in the cell extract were separated as described earlier [17,18]. Briefly, immobilized pH gradient-isoelectric focusing (IPG-IEF) in the first-dimension was performed on a Immobiline DryStrip gel, pH 4–7, 18 cm in length (Bio-Rad), in a CoolPhoreStar Model 3610 Horizontal IEF apparatus (Anatech, Tokyo, Japan). Aliquots of 40 μg of protein lysate per gel were loaded. After electrofocusing at 46,700 Vh, SDS-PAGE was performed vertically in a Tris–Tricine buffer system using a CoolPhoreStar model 3068 electrophoresis apparatus (Anatech). Proteins on gels were visualized by staining with SYPRO Ruby (Molecular Probes, Eugene, OR).

### 2.5. Evaluation of protein patterns

Two-dimensional gel images were scanned at an excitation wavelength of 488 nm, and emission wavelengths over 550 nm were collected on a Molecular Imager FX (Bio-Rad) as described earlier [18]. Noise reduction, background subtraction, normalization, and quantitative profiling of proteins in 2-DE gels were carried out using PDQuest software version 8.0 (Bio-Rad). Experiments were performed in triplicate using three separate samples from independent cultures. Student's *t* test was used to determine the significance of stage-to-stage differences. Novel spots that appeared at a later stage were included in the comparison as increasing spots.

Author's personal copy



*2.6. Mass spectrometry*

In-gel digestion and MS analysis were carried out as described earlier [17,18]. Briefly, MS analysis was performed on a MALDI-TOF mass spectrometer (AXIMA-CFR; Shimadzu, Kyoto, Japan) in reflectron mode. Protein spots were identified by matching all the peptide masses against the Swiss-Prot using Mascot search (http://www.matrixscience.com/search form select.htmL). For LC-MS-MS analysis, the tryptic peptides were separated using a DiNa direct nano HPLC system (KYA Technologies, Tokyo, Japan) with a gradient of buffer A (2% acetonitrile containing 0.1% formic acid) and buffer B (80% acetonitrile containing 0.1% formic acid) by two-step linear gradient elution. The eluted peptides were injected directly into Q-TOF MS (Q-TOF Synapt; Waters, Milford, MA) through a nano-LC probe (ESI). The collision gas used was argon. ProteinLynx Global Server version 2.3 (Waters) was used to create and search files with the Mascot search engine (version 2.2.04; Matrix Science) for peptide and protein identification. Search parameters were as follows: trypsin digestion allowing one missing cleavage, carbamidomethylation at cysteine residues as fixed modifications, oxidation at methionine residues as variable modifications, +2 and +3 peptide charge, peptide mass tolerance of 30 ppm, and MS/MS fragment tolerance of 0.15 Da were used for all the tryptic-mass searches. Samples with total ion scores of less than 45 were rejected. The protein names and accession numbers are reported based on SwissProt 56.0.

*2.7. Western blotting analysis*

Following SYPRO Ruby-staining, each 2-DE gel was washed three times with Milli-Q water for 30 min each time. Each gel was incubated in 25 mM Tris/93 mM glycine/0.2% SDS for 15 min to resolubilize proteins, and the proteins were transferred onto PVDF membranes (Millipore, Bedford, MA) using a semi-dry electroblotting apparatus at *ca.* 2 mA/cm$^2$ for 1 h at room temperature in a buffer containing 25 mM Tris, 192 mM glycine, 0.08% SDS, and 20% methanol. The blotted membranes were rinsed twice with 10 mM Tris–HCl/150 mM NaCl/1 mM $CaCl_2$/1 mM $MgCl_2$, pH 7.4 (TBS), and blocked with 3% ECL blocking agent (GE Healthcare Biosciences)/0.05% Tween-20/TBS (T-TBS) for 1 h. The membranes were rinsed twice with T-TBS and incubated with primary antibody overnight at 4 °C. The following primary antibodies were used: anti-FABP7 (rabbit anti-FABP7 polyclonal antibody, ab9558, 1:5000; Millipore); anti-CRABP1 (rabbit anti-cellular retinoic acid binding protein 1 polyclonal antibody, ab2816, 1:5000; Abcam, Cambridge, UK); anti-CRMP2 (rabbit anti-dihydropyrimidinase-related protein 2 polyclonal antibody, ab62661, 1:50,000; Abcam); anti-pCRMP2-T514 (rabbit anti-CRMP2 phosphorylated on Thr514 polyclonal antibody, ab85934, 1:5000; Abcam), and anti-pCRMP2-S522 (rabbit anti-CRMP2 phosphorylated on Ser522 polyclonal antibody, CP2191, 1:500; ECM Biosciences, Versailles, KY). After washing three times with T-TBS, the membranes were incubated with appropriate horseradish peroxidase-conjugated secondary antibody (goat anti-rabbit IgG, A 6154, 1:5000; Sigma), followed by assay using the ECL Western blotting Detection System (GE Healthcare Biosciences).

*2.8. Quantitative real-time RT-PCR*

Poly(A)$^+$ mRNA was prepared from undifferentiated ES colonies, Day 4 cells, NSS cells, NS cells, and AstP cells using QuickPrep Micro mRNA Purification Kits (GE Healthcare Biosciences). Each mRNA was reverse transcribed into cDNA using random hexamer primers, in accordance with the manufacturer's instructions (Applied Biosystems, Foster City, CA). Quantitative real-time RT- PCR was performed on an ABI PRISM 7300 (Applied Biosystems) using SYBR Green PCR Master Mix and the primer pairs shown in Supplementary Table 1, which had been designed using Primer Express software (Applied Biosystems), in accordance with the manufacturer's instructions. Expression of each target gene was normalized relative to that of GAPDH mRNA, with relative quantitative evaluation of the initial template copy number determined relative to a standard curve of GAPDH cDNA (Applied Biosystems). All samples were analyzed in five replicates. Student's *t* test was used to determine the significance of stage-to-stage differences in the same manner as described in Section 2.5.

*2.9. Searches of protein–protein interactions and metabolic pathways related to identified proteins*

Protein interaction maps of the differentially expressed proteins were explored using STRING (http://string.embl.de/) based on reported protein–protein interactions. Next, the differentially expressed protein-interacting proteins with STRING scores $\geq 0.75$ were extracted. The metabolic pathways related to the differentially expressed proteins and their interacting proteins were then searched using the KEGG pathway against human databases (http://www.genome.jp/kegg/tool/map_pathway1.htmL), as there was less information in monkey databases, and monkey shares many physiological similarities with humans.

## 3. Results

*3.1. Differential protein expression during differentiation from ES cells to AstP cells*

To identify proteins that may be differentially regulated during differentiation from ES cells to AstP cells, we differentiated monkey ES cells (CMK6 clone) to primitive NSS cells by culturing in ACM for 4 days (Day 4 cells). Primitive NSS displayed peripheral immature NS cells with a center of proliferating ES cells as reported previously [9,10,12,13]. After culture in ACM for 4 days, proliferation of primitive NSS cells increased and expression levels of ES cell markers, Oct-3/4 and Nanog mRNA, decreased to 7.8% and 14.6% of the expression levels of ES cells, respectively. Whereas the monkey ES cells expressed undifferentiated ES cell-marker genes, such as Oct4, Nanog, and Cripto mRNA as reported previously [14]. Immunostaining indicated that the ES cells expressed Oct4, SSEA-1, Nanog, and alkaline phosphatase as reported previously [14]. The levels of expression of Pax 6, MAP2, and GFAP in ES cells by RT-PCR were 0.0%, 0.3%, and 0 %, respectively, as reported previously [14]. Subsequently, we differentiated these cells into mature NSS cells by culturing in ACM for 12 days (NSS cells). The mature NSS showed peripheral NS cells with a center of ES cells as reported earlier [9,10,12,13]. We differentiated mature NSS to highly homogeneous NS cells by culturing NSS in Neurobasal medium supplemented with B-27, FGF-2, and EGF on an adhesive substrate. Then, circular clusters of cells were formed, from which many Nestin-positive NS cells migrated. The migrated NS cells expressed Nestin (99.5% ± 0.5%) and only a few cells (<0.5%) expressed NF-H as reported earlier [14]. The NS cells were immunoreactive for neither antibody against the astrocyte marker GFAP nor the antibody against oligodendrocyte protein O4 as reported earlier [14]. RT-PCR showed that the relative levels of expression of Pax 6, MAP2 and GFAP in NS cells were 100%, 4.6% and 0%, respectively, as reported earlier [14]. Next, NS cells were induced to differentiate into astrocytes by culturing without FGF-2 and EGF for 7 days. After culture for 7 days, the relative levels of GFAP, Nestin, MAP2 mRNA expression in the differentiated cells were 100%, 10%, and 12%, respectively, which were similar to those in mouse [11]. Fig. 1 indicates the phase-contrast micrograph of monkey ES cells (Fig. 1A), Day 4 cells (Fig. 1B), NSS cells (Fig. 1C), NS cells (Fig. 1D), AstP cells (Fig. 1E and F), and immunofluorescence analysis of the AstP cells (Fig. 1G). As shown in Fig. 1G, the monkey cells after culture without FGF-2 and EGF for 7 days indicated partial GFAP protein expression (68.3 ± 4.1%). The corresponding mouse cells by culturing NS cells without FGF-2 and EGF for 7 days (mouse astrocytes) show GFAP protein expression (90.0% ± 3.7%) [11], and human astrocytes by culturing NS cells without FGF-2 and EGF for 14 days show GFAP protein

Author's personal copy



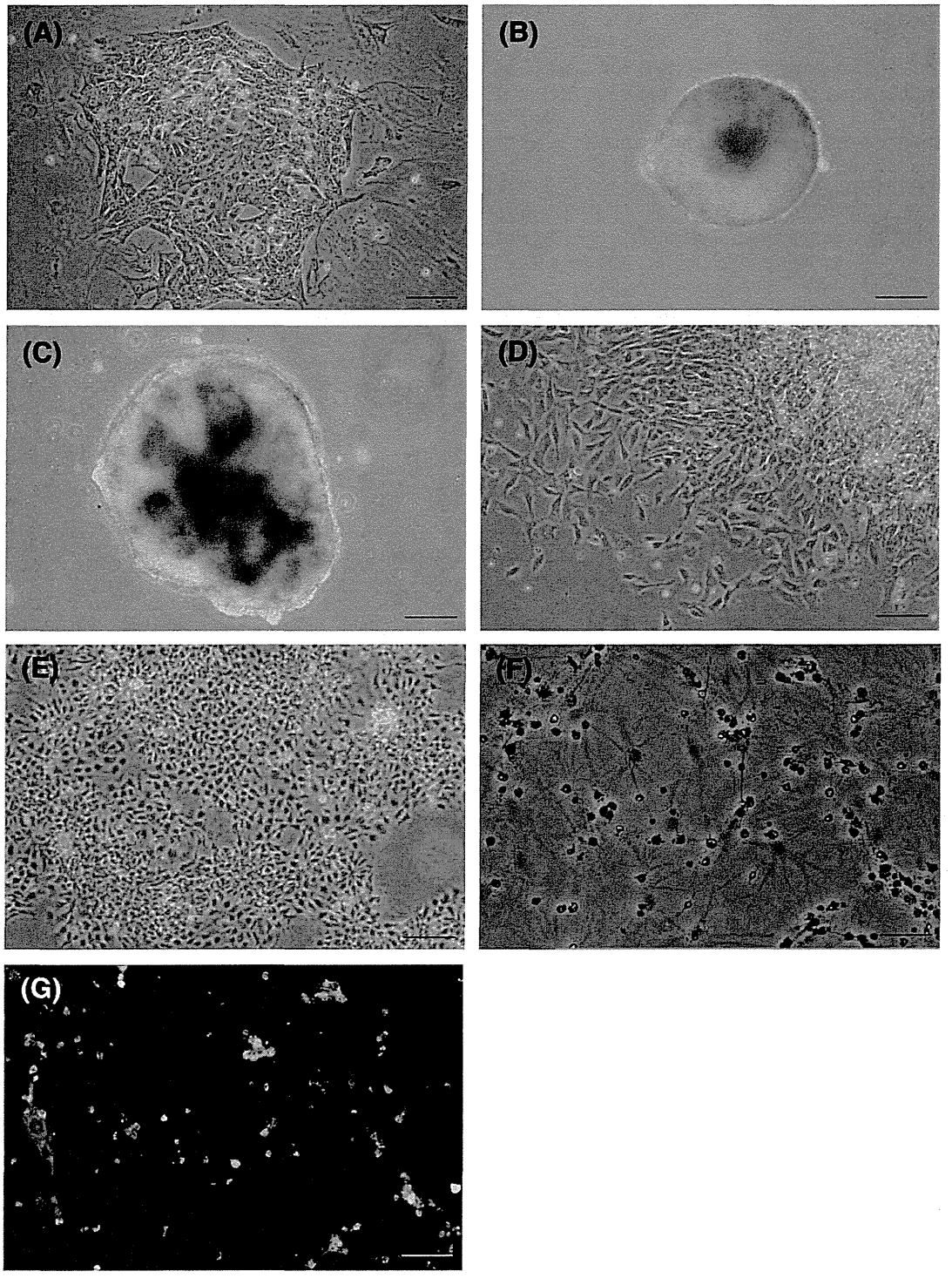



**Fig. 1.** Differentiation of monkey ES cells to AstP cells. Phase-contrast micrographs showing monkey ES cells (A), Day 4 cells (B), NSS cells (C), NS cells (D), AstP cells (E). (F and G) High magnification images of panel (E). (G) GFAP (green) staining profile by fluorescence microscope analysis of panel (F). Scale bars: (A–E) 100 μm, (F and G) 50 μm. (For interpretation of the references to color in this figure legend, the reader is referred to the web version of this article.)

expression (82.4 ± 1.8%) [15]. These discrepancies may be due to about twice slower differentiation of monkey cells as well as human cells [15] than that of mouse cells. Therefore, the monkey cells with partial GFAP protein expression were considered to be on the way of differentiation from NS cells to mature astrocytes. Accordingly, these monkey cells were designated as AstP cells.

We used an IPG strip gel of pH 4–7 as the first step, which had a higher resolution at pH 4–7 than the strip gel of pH 3–10. Approximately 500 protein spots were detected by SYPRO Ruby staining. We obtained reproducible 2-DE profiles and relative spot intensities from all samples in experiments performed in triplicate. Fig. 2 shows typical gel maps of proteins from monkey ES cells, Day 4 cells, NSS cells, NS cells, and AstP cells. To assess changes in protein patterns among these five stages, we compared the patterns of ES cells and Day 4 cells, the patterns of Day 4 cells and NSS cells, the patterns of NSS cells and NS cells, and the patterns of NS cells and AstP cells. The relative intensities of the corresponding spots in two stages are shown in Table 1 and Supplementary Table 2. These differentially expressed proteins were selected for subsequent

Author's personal copy



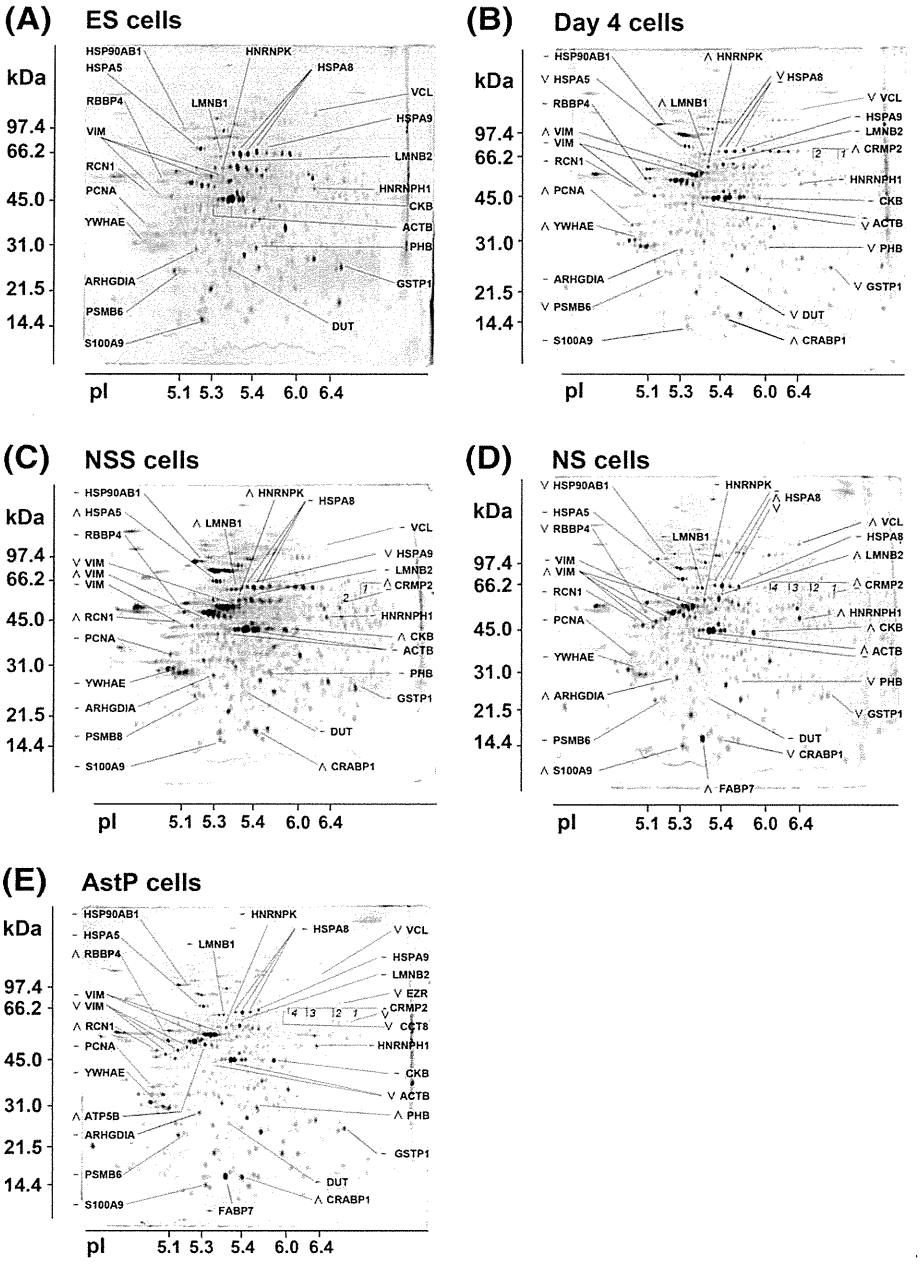



**Fig. 2.** 2-DE protein profiles from monkey (A) ES cells, (B) Day 4 cells, (C) NSS cells, (D) NS cells, and (E) AstP cells. Proteins were separated based on pI (x-axis) and molecular mass (y-axis), and visualized by staining with SYPRO Ruby. Each protein was identified by PMF and LC-MS-MS, and identified proteins with altered expression are shown on the gels. (∧) and (∨) indicate up- and down-regulated proteins, respectively. (−) Unaltered proteins.

analysis by MS. Peptide mass fingerprinting (PMF) and LC-MS-MS of the selected spots followed by a database search revealed the identities of these proteins (Table 1 and Supplementary Table 3). The possible functions of the differentially regulated proteins during differentiation from ES cells to AstP cells are listed in Supplementary Table 4.

Of the metabolism-related proteins, dUTP pyrophosphatase (DUT) was downregulated in Day 4 cells. CRABP1 was found to be upregulated in Day 4 cells and in NSS cells followed by its downregulation in NS cells. Then, CRABP1 was re-upregulated in AstP cells. On the other hand, fatty acid binding protein 7 (FABP7), a marker of NS cells, was upregulated from NSS cells to NS cells. Of the heat shock/stress proteins, T-complex protein subunit theta (CCT8) was downregulated in AstP cells. Of the cytoskeletal proteins, vimentins (VIM) were upregulated in Day 4 cells, NSS cells, and NS cells, but a few were downregulated in AstP cells. Ezrin (EZR) was downregulated in AstP cells. Vinculin (VCL) involved in cell adhesion was downregulated in Day 4 cells, upregulated in the adherent culture of NS cells, followed by its downregulation in AstP cells. Of the signal transduction-related proteins, NSS cells and AstP cells showed upregulation of reticulocalbin 1 (RCN1), which is thought to be involved in calcium signal modulation based on its amino acid sequence with four EF hands (http://www.geneontology.org/). We observed four spots of collapsing response mediator protein 2 (CRMP2) (Fig. 2 and Table 1). Based on their electrophoretic mobilities on 2-D gels [18,19], spots 1, 2, 3, and 4 of CRMP2 were thought to be nonphosphorylated CRMP2 (CRMP2-1), CRMP2 phosphorylated at Ser 522 (CRMP2-2), CRMP2 phosphorylated at Ser 522 and Thr 514 (CRMP2-3), and CRMP2 phosphorylated at Ser 522, Thr 514, and Thr 509/Ser 518 (CRMP2-4), respectively. CRMP2-1 was upregulated in Day 4 cells and in NSS cells, but downregulated in AstP cells. CRMP2-2 was upregulated in Day 4 cells and in NS cells. CRMP2-3 and CRMP2-4 were upregulated during differentiation from NSS cells to NS cells. Of the cell cycle-related proteins, retinoblastoma binding protein 4 (RBBP4), which is involved in DNA

Author's personal copy



**Table 1**
Differentially expressed proteins of monkey Day 4 cells, NSS cells, NS cells, and AstP cells differentiated from ES cells by the NSS method.

| Protein name | Ssp No.[a] | Quantitative changes[b] | | | | Accession number [g] | Mowse score [h] | Matched peptides [i] | Sequence cov. (%) [j] |
|---|---|---|---|---|---|---|---|---|---|
| | | Day 4 cells [c] | NSS cells[d] | NS cells [e] | AstP cells[f] | | | | |
| *DNA metabolism* | | | | | | | | | |
| Proliferating cell nuclear antigen (PCNA) | 1305 | 1.84 (0.05) | – | – | – | P12004 | 68/424 | 5/12 | 17/48 |
| dUTP pyrophosphatase (DUT) | 4210 | −0.45 (0.05) | – | – | – | P33316 | 91/272 | 6/6 | 53/27 |
| *RNA metabolism* | | | | | | | | | |
| Heterogeneous nuclear ribonucleoprotein K (HNRNPK)[k] | 4503 | 1.37 (0.05) | 1.18 (0.05) | – | – | Q3T0D0 | 518 | 13 | 24 |
| Heterogeneous nuclear ribonucleoprotein H1 (HNRNPH1) | 7404 | – | – | 2.00 (0.05) | – | P31943 | 74/448 | 7/9 | 20/29 |
| *Protein metabolism* | | | | | | | | | |
| Proteasome subunit beta type-6 (PSMB6)[k] | 2203 | −0.58 (0.01) | – | – | – | P28073 | 95 | 2 | 10 |
| *Lipid metabolism* | | | | | | | | | |
| Fatty acid binding protein 7 (FABP7) | 4201 | NA [l] | NA [l] | ▲ (0.05) | – | Q15540 | 169/222 | 10/4 | 83/34 |
| Cellular retinoic acid binding protein 1 (CRABP1) | 5201 | ▲ (0.05) | 3.47 (0.01) | −0.31 (0.01) | 3.26 (0.05) | P29762 | 119/263 | 6/8 | 48/46 |
| *Energy metabolism* | | | | | | | | | |
| ATP synthase subunit bet (ATB5B) | 3401 | – | – | – | 1.33 (0.05) | P06576 | 135/1313 | 12/26 | 40/48 |
| Creatine kinase B type (CKB) | 6306 | – | 2.44 (0.01) | 1.26 (0.05) | – | P12277 | 154/357 | 14/9 | 43/24 |
| *Signal transduction* | | | | | | | | | |
| 14-3-3 Protein epsilon (YWHAE)[k] | 1304 | 1.88 (0.01) | – | – | – | Q5ZMT0 | 492 | 13 | 37 |
| Reticulocalbin 1 (RCN1) | 1402 | – | 4.70 (0.05) | – | 1.58 (0.05) | Q15293 | 70/94 | 6/2 | 17/8 |
| CRMP 2-1[m] | 8503 | ▲ (0.05) | 4.30 (0.01) | – | −0.37 (0.05) | Q5R9Y6 | 121/287 | 12/8 | 25/18 |
| CRMP 2-2[n] | 7506 | ▲ (0.05) | – | 3.20 (0.05) | – | Q5R9Y6 | 211/237 | 18/6 | 41/16 |
| CRMP 2-3[o] | 7603 | NA [l] | NA [l] | ▲ (0.05) | – | Q5R9Y6 | 108/188 | 9/6 | 21/16 |
| CRMP 2-4[p] | 6614 | NA [l] | NA [l] | ▲ (0.05) | – | OD8553 | 63/356 | 5/9 | 13/21 |
| Rho GDP-dissociation inhibitor 1 (ARHGDIA) | 2206 | – | – | 1.55 (0.01) | – | Q4R4J0 | 129/256 | 9/7 | 38/25 |
| Protein S-100-A9 (S100A9)[k] | 3201 | – | – | 1.69 (0.01) | – | P06702 | 415 | 8 | 66 |
| *Heat shock/stress proteins* | | | | | | | | | |
| 78 kDa glucose-regulated protein (HSPA5) | 2604 | −0.56 (0.05) | 1.68 (0.05) | – | – | P11021 | 154/870 | 14/25 | 29/38 |
| HSP 90-β1 (HSP90AB1) | 2702 | – | – | −0.45 (0.05) | – | Q4R520 | 83/242 | 14/5 | 20/9 |
| Heat shock cognate 71 kDa protein (HSPA8) | 4611 | −0.64 (0.01) | – | – | – | A2Q0Z1 | 84/382 | 7/11 | 13/22 |
| Heat shock cognate 71 kDa protein (HSPA8) | 5602 | – | – | 1..32 (0.01) | – | A2Q0Z1 | 244/1340 | 25/36 | 42/35 |
| Heat shock cognate 71 kDa protein (HSPA8) | 5606 | – | – | −0.64 (0.05) | – | A2Q0Z1 | 66/413 | 6/10 | 11/20 |
| Stress-70 protein (HSPA9) [k] | 5609 | – | −0.81 (0.05) | – | – | Q5R511 | 854 | 18 | 33 |
| T-complex protein 1 subunit theta (CCT8)[k] | 6502 | – | – | – | −0.65 (0.05) | Q4R5J0 | 945 | 22 | 45 |
| Glutathione S-transferase P (GSTP1) | 8203 | −0.60 (0.01) | – | −0.64 (0.01) | – | Q28514 | 66/159 | 4/4 | 27/20 |
| *Cytoskeleton* | | | | | | | | | |
| Vimentin (VIM) | 1404 | – | – | 6.96 (0.01) | −0.58 (0.01) | Q4R4X4 | 213/1155 | 20/31 | 48/48 |
| Vimentin (VIM) | 2401 | NA [l] | NA [l] | ▲ (0.05) | −0.46 (0.01) | Q4R4X4 | 304/861 | 30/25 | 64/48 |
| Vimentin (VIM) | 2403 | NA [l] | ▲ (0.05) | 7.49 (0.01) | −0.55 (0.01) | Q4R4X4 | 354/363 | 34/10 | 71/24 |
| Vimentin (VIM) | 3501 | – | 1.38 (0.05) | – | – | Q4R4X4 | 165/823 | 13/23 | 33/51 |
| Vimentin (VIM) | 3508 | 5.54 (0.05) | −0.20 (0.05) | 3.60 (0.05) | – | Q4R4X4 | 171/492 | 13/15 | 39/28 |
| Actin cytoplasmic 1 (ACTB) | 3306 | −0.15 (0.01) | – | – | −0.21 (0.01) | Q4L0Y2 | 79/155 | 8/6 | 28/21 |
| Actin cytoplasmic 1 (ACTB) | 4404 | – | – | 1.39 (0.05) | −0.79 (0.01) | Q4L0Y2 | 170/795 | 15/20 | 36/51 |
| Lamin B1 (LMNB1) | 4602 | 1.30 (0.05) | 1.26 (0.05) | – | – | P20700 | 107/427 | 11/15 | 19/19 |
| Lamin B2 (LMNB2) | 5603 | – | – | 2.73 (0.05) | – | Q03252 | 151/231 | 21/6 | 35/12 |
| Vinculin (VCL) | 7703 | −0.25 (0.05) | – | 8.90 (0.01) | −0.20 (0.01) | P18206 | 85/635 | 14/18 | 15/21 |
| Ezrin (EZR) | 8601 | – | – | – | −0.26 (0.05) | P15311 | 89/170 | 10/4 | 15/9 |

Author's personal copy



**Table 1** (*continued*)

| Protein name | Ssp No.[a] | Quantitative changes[b] | | | | Accession number[g] | Mowse score[h] | Matched peptides[i] | Sequence cov. (%)[j] |
|---|---|---|---|---|---|---|---|---|---|
| | | Day 4 cells[c] | NSS cells[d] | NS cells[e] | AstP cells[f] | | | | |
| *Cell cycle* | | | | | | | | | |
| Prohibitin (PHB) | 5207 | −0.57 (0.05) | − | −0.58 (0.05) | 2.13 (0.01) | Q3T165 | 238/159 | 16/3 | 58/15 |
| Retinoblastoma binding protein 4 (RBBP4) | 1502 | − | − | −0.48 (0.05) | 2.79 (0.01) | Q3MHL3 | 62/401 | 6/9 | 15/27 |

[a] Special spot number on 2-DE gel (Fig. 2) obtained using PDQuest software version 8.0 (Bio-Rad).
[b] The values show the fold-increase of proteins toward the older developmental stage. The minus values (−) show their fold-decrease. Novel protein spots that appeared at a later stage were included in the comparison as increasing spots, and their upregulation is shown by (▲). (−): No change.
[c] ES cells vs. Day 4 cells. For protein spots that showed statistical significance, the *P*-values are shown in parentheses (*t* test).
[d] Day 4 cells vs. NSS cells. For protein spots that showed statistical significance, the *P*-values are shown in parentheses (*t* test).
[e] NSS cells vs. NS cells. For protein spots that showed statistical significance, the *P*-values are shown in parentheses (*t* test).
[f] NS cells vs. AstP cells. For protein spots that showed statistical significance, the *P*-values are shown in parentheses (*t* test).
[g] Swiss-Prot accession numbers are given for proteins.
[h] Score resulted from PMF/LC-MS-MS search (http://www.matrixscience.com/search_form_select.html). Score in PMF is −10*Log(P), where P is the probability that the observed match is a random event. Protein scores greater than 61 are significant ($p<0.05$). In LC-MS-MS search, ion score is −10*Log(P), where P is the probability that the observed match is a random event. Individual ion scores >35 indicate identity or extensive homology ($p<0.05$). Protein score are derived from ions sores as a non-probabilistic basis for ranking protein hits.
[i] Numbers of matched peptides that resulted from PMF/those that resulted from LC-MS-MS search obtained using the Mascot search engine.
[j] Sequence coverage that resulted from PMF/that resulted from LC-MS-MS search.
[k] Identified by LC-MS-MS search.
[l] NA: not detectable on the gel (<1.7 pmol).
[m] Spot 1 of CRMP2 in Fig. 2.
[n] Spot 2 of CRMP2 in Fig. 2.
[o] Spot 3 of CRMP2 in Fig. 2.
[p] Spot 4 of CRMP2 in Fig. 2.

replication, cell cycle, regulation of transcription, and chromatin modification, was downregulated in NS cells, but upregulated in AstP cells.

### 3.2. Comparison of protein and mRNA expression levels

To investigate the expression levels of the mRNAs encoding the identified proteins, we performed real-time RT-PCR analyses for DUT, VCL, CRABP1, RCN1, RBBP4, EZR, CRMP2, and FABP7 (Supplementary Table 5). Fig. 3 shows a comparison of protein and mRNA expression. The levels of RCN1 and CRMP2 mRNA expression in NSS cells (Fig. 3D and G), those of VCL, CRABP1, RBBP4, CRMP2, and FABP7 mRNA in NS cells (Fig. 3B, C, E, G, and H), and those of VCL, CRABP1, and RBBP4 mRNA in AstP cells (Fig. 3B, C, and E) showed alterations similar to those of the respective protein expression levels. However, the expression patterns of other proteins and their mRNAs in the other differentiation stages were not similar. We also found that the levels of CRMP2, CRABP1, and EZR mRNA expression were unchanged from ES cells to Day 4 cells (Fig. 3G), from Day 4 cells to NSS cells (Fig. 3C), and from NS cells to AstP cells (Fig. 3F), respectively, in contrast to the changes in expression levels of the encoded proteins.

We found that the CRABP1 and CRMP2 mRNA and protein expression patterns were not completely similar (Fig. 3C and G). These proteins are of interest in that they are thought to be involved in regulating neural differentiation [20,21]. To confirm the differential expression of CRABP1 and CRMP2, we performed 2-D western blotting analyses of these proteins, together with FABP7 as a marker protein of NS cells, using the same specimens as used for 2-DE (Fig. 4). The results of Western blotting analysis were consistent with the data obtained by 2-DE except for the increases in CRMP2-3 and CRMP2-4 expression in NSS cells (Fig. 4C), which were not detected by SYPRO Ruby staining (Table 1 and Fig. 3G), possibly due to the lower sensitivity of the latter method. Comparisons of protein and mRNA expression levels suggested that the upregulation of CRABP1 protein in Day 4 and NSS cells as well as the upregulation of CRMP2-1 and CRMP2-2 in Day 4 cells and the downregulation of CRMP2-1 in AstP cells also occurred at the post-transcriptional level.

Phospho-CRMP2 immunoblotting of NS cells (Fig. 4D) indicated that CRMP2-1, CRMP2-2, and CRMP2-3 were nonphosphorylated, monophosphorylated on Ser 522, and diphosphorylated on Thr 514 and Ser 522, respectively, and suggested that CRMP2-4 was triphosphorylated on Thr 514, Ser 522, and X (undetermined amino acid residue).

### 3.3. Metabolic pathways estimated from the identified proteins and their interacting proteins

Protein–protein interaction networks of the identified proteins with altered expression were explored using the search tool STRING. The identified protein-interacting proteins in Day 4 cells, NSS cells, NS cells, and AstP cells with STRING scores ≥0.75 were extracted as shown in Supplementary Tables 6–9, respectively. Metabolic pathways related to the differentially expressed proteins and their interacting proteins were searched using the KEGG pathway. The representative metabolic pathways included apoptosis in Day 4 cells, NSS cells, NS cells, and AstP cells (Supplementary Fig. 2A–D), axon guidance in Day 4 cells and NS cells (Supplementary Fig. 2E and F), Notch signaling in NS cells (Supplementary Fig. 2G), focal adhesion in AstP cells (Supplementary Fig. 2H), and regulation of actin cytoskeleton in AstP cells (Supplementary Fig. 2I).

## 4. Discussion

### 4.1. Differential protein expression during differentiation from ES cells to AstP cells

The present study was performed to examine differentially regulated proteins during the differentiation of monkey ES cells into AstP cells, using the differentiation system from ES cells to AstP cells *via* the formation of NSS and NS cells.

Some of the proteins identified here to be differentially expressed from ES cells to AstP cells have been reported to be differentially regulated in mammalian early neurogenesis [18,22–35] (Supplementary Table 4). From NS cells to AstP cells, FABP7 protein, a marker of NS cells, was found to remain unchanged, however its mRNA was downregulated (Table 1, Figs. 3H and 4A), whereas protein and mRNA of FABP7 have been shown to remain unchanged from NS cells to neurons [18]. RCN1 was found to be upregulated in NSS cells, and further in AstP cells as well as in neurons [18], however its mRNA was downregulated in NS cells and in AstP cells (Fig. 3D). CRMP2 is known to be related to nervous system disorders including schizophrenia and

Author's personal copy



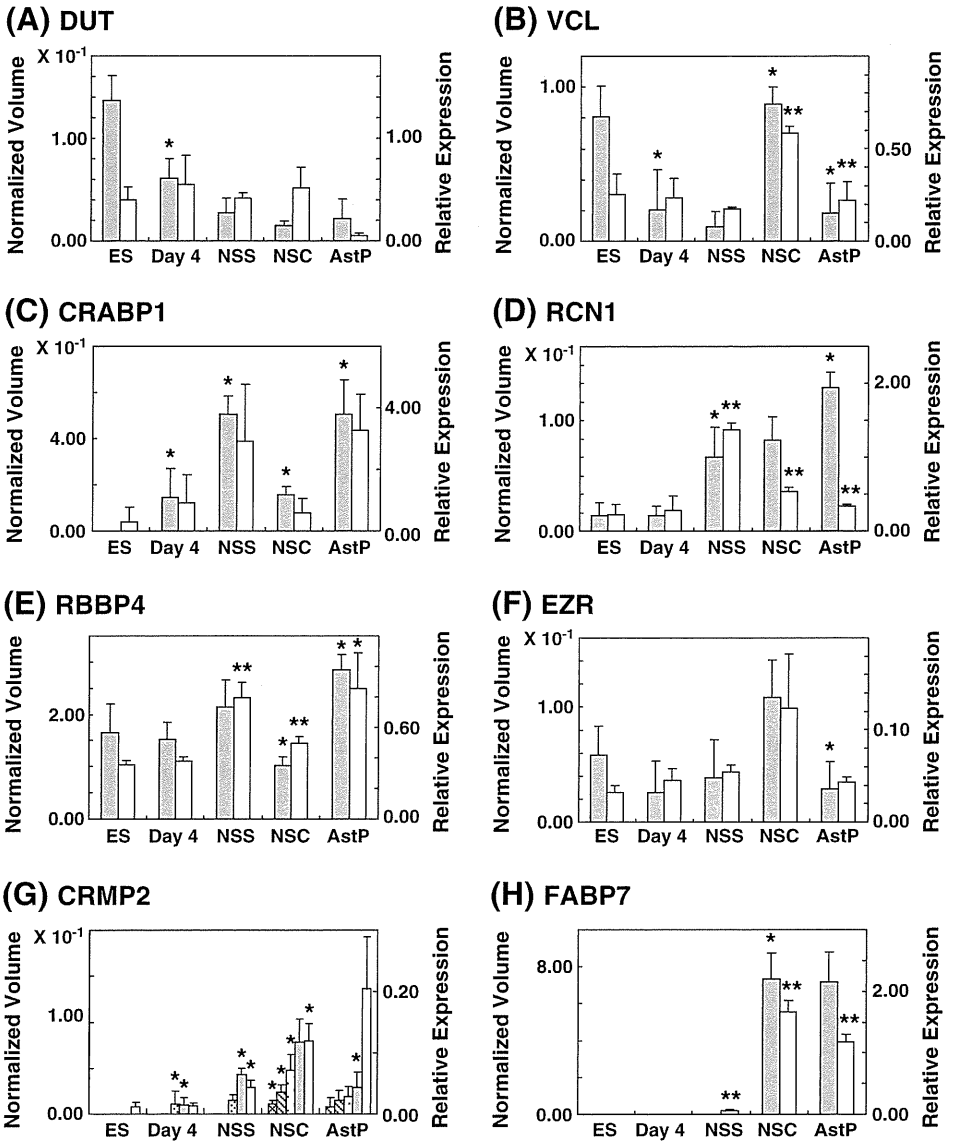



**Fig. 3.** Protein and RNA expression of eight identified genes. RNA expression assayed by real-time RT-PCR and protein expression assayed by 2-DE are plotted for each stage of differentiation (ES cells, Day 4 cells, NSS cells, NS cells, and AstP cells). (A–F, H): White bars indicate RNA expression, whereas gray bars indicate protein expression. (G): White bars refer to RNA expression; Gray, dotted, slanted stripes, and checked-bars refer to expression of the proteins CRMP2-1, CRMP2-2, CRMP2-3, and CRMP2-4, respectively. The vertical axis on the left shows the normalized volume of each protein spot on 2-DE, and that on the right shows the relative amounts of RNA normalized relative to the signals for the ubiquitously expressed GAPDH mRNA. ES, ES cells; Day 4, Day 4 cells; NSS, NSS cells; NSC, NS cells; AstP, AstP cells. *$P<0.05$, **$P<0.01$ for comparisons of the corresponding expression at two stages.

Alzheimer's disease [36,37]. CRMP2-1 (nonphosphorylated CRMP2) was found to be upregulated in Day 4 cells and NSS cells, but downregulated from NS cells to AstP cells, (Table 1, Fig. 3G, and Fig. 4C and D), whereas CRMP2-1 has been shown to remain unchanged from NS cells to neurons [18]. CRMP2-2 (thought to be CRMP2 phosphorylated at Ser 522) was upregulated in Day 4 cells and NS cells, whereas CRMP2-2 has been shown to be further upregulated in neurons [18]. CRMP2-3 (thought to be CRMP2 phosphorylated at Thr 514 and Ser 522) and CRMP2-4 (thought to be CRMP2 phosphorylated at Thr 514, Ser 522, and X) were upregulated in NSS cells and NS cells, and remained unchanged in AstP cells (Table 1, Fig. 3G and Fig. 4C and D), whereas CRMP2-4 has been shown to be further upregulated in neurons [18]. The findings that interaction between CRMP2 and tubulin is altered by CRMP2 phosphorylation, by Cdk5 as a priming kinase at Ser 522, and by GSK-3β at Thr 514, inhibiting axon outgrowth [38–43] supported our observation on CRMP2s. Collectively, these results suggest that the functions of AstP cells are similar but different from those of NS cells and neurons.

The importance of retinol (vitamin A) in the form of retinoic acid in the developing neural tube has been demonstrated by studies in transgenic mouse and zebra fish models [44,45]. All-*trans* retinoic acid is used extensively to promote neurogenesis *in vitro* [24,34,46]. CRABP1 is thought to facilitate catabolism and/or sequestering of retinoic acid, rendering it unavailable to nuclear receptors [47], whereas CRABP2 facilitates the transfer of all-*trans* retinoic acid to nuclear receptor, allowing the subsequent binding to retinoic acid response elements in certain target genes and their activation [46]. We found that protein expression of CRABP1 was upregulated in Day 4 cells and NSS cells, downregulated in NS cells, and re-upregulated in AstP cells, and that its mRNA was also downregulated in NS cells, and re-upregulated in AstP cells (Table 1, Figs. 3C and 4B), whereas protein and mRNA expression of CRABP1 has been shown to remain unchanged in neurons [18]. The level of CRABP2 protein was not altered, although its mRNA expression was upregulated in NSS cells, downregulated in NS cells, and remained unchanged in AstP cells (Supplementary Table 5). On the other hand, DUT was downregulated during differentiation from ES

Author's personal copy



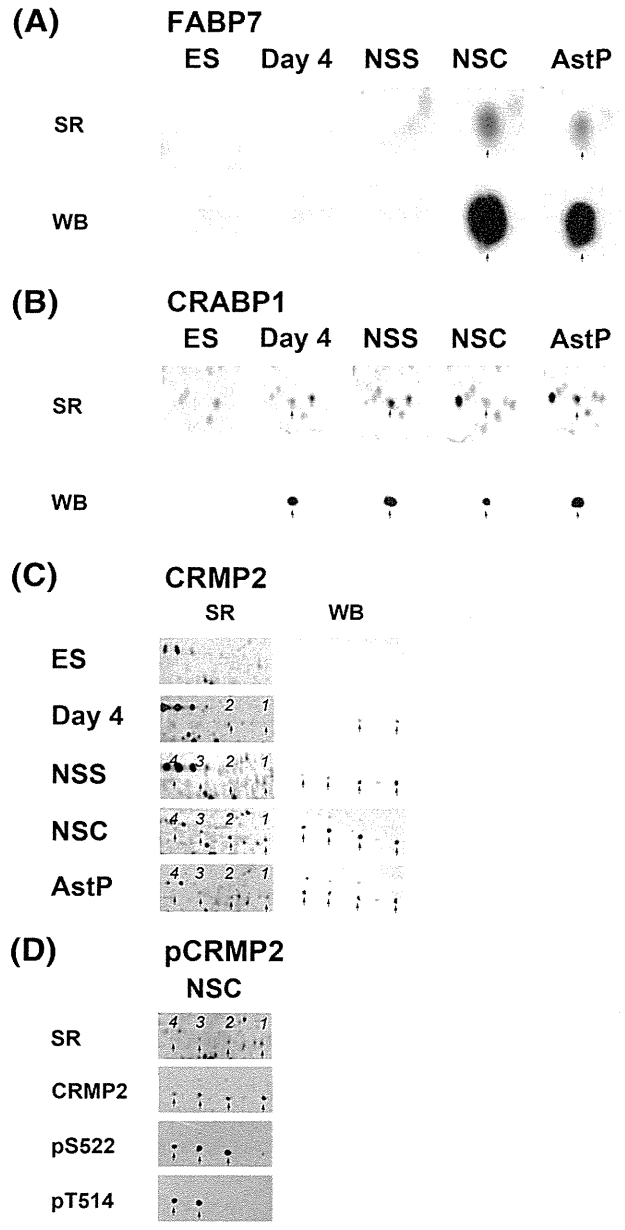



**Fig. 4.** 2-DE Western blotting analysis of a typical enlarged portion from 2-D gel electrophoretic gel from ES cells, Day 4 cells, NSS cells, NS cells, and AstP cells. Proteins were visualized by staining with SYPRO Ruby, and by Western blotting analysis with the following antibodies: (A) anti-FABP7, (B) anti-CRABP1, (C) anti-CRMP2, and (D) anti-CRMP2 (CRMP2), anti-CRMP2 phosphorylated on Ser-522 (pS522), anti-CRMP2 phosphorylated on Thr-514 (pT514), to detect phosphorylated CRMP2 (pCRMP2). Western blotting analysis of 2-DE gels was performed as described in Materials and methods section. ES, ES cells; Day 4, Day 4 cells; NSS, NSS cells; NSC, NS cells; AstP, AstP cells.

cells to Day 4 cells (Table 1 and Fig. 3A). DUT has been reported to prevent peroxisome proliferator-activated receptor (a member of the nuclear receptor superfamily)–retinoid X receptor heterodimerization resulting in inhibition of the receptor activity in a ligand-independent manner [48]. As outlined in Supplementary Fig. 3, these findings suggest that in ES cells DUT is involved in inhibiting gene activation by retinoic acid; in Day 4 cells and NSS cells, the increased CRABP1 controls retinoic acid concentration and the gene activation by retinoic acid; the decrease in CRABP1 expression promotes the activation of genes necessary for differentiation from NSS cells to NS cells; the re-increase in CRABP1 expression regulates the gene activation by retinoic acid to promote differentiation of NS cells to AstP cells. It has been reported that there is tight regulation of retinoic acid levels in the mouse embryo and specific distributions of retinoic acid-synthesizing and retinoic acid-metabolizing enzymes [49], and disruption of this balance leads to birth defects, including neural tube defects [50]. Taken together, our results suggest that CRABP1 is involved in the tight regulation of retinoic acid concentration and gene activation during monkey differentiation of ES cells into AstP cells with its rhythmic increases and decrease. Protein interaction maps of the differentially expressed proteins using the search tool STRING have suggested that CRABP1 is a date hub, connecting modules such as regulators, mediators, and adaptors [18]. Investigating the mechanisms by which CRABP1 expression is regulated may be important for understanding the differentiation of primate ES cells to AstP cells.

### *4.2. Metabolic pathways related to differentially regulated proteins*

A search using KEGG of the metabolic pathways related to the differentially expressed proteins and their interacting proteins suggested that apoptosis-associated proteins, such as caspases 3, 6, 7, and p53, were more closely related to differentiation from monkey ES cells to Day 4 cells and NSS cells than from NSS to NS cells and AstP cells (Supplementary Fig. 2A–D). During the differentiation from monkey ES cells to NSS cells, selective apoptosis of non-neuronal cells was not detected using TUNEL assays (data not shown). Mouse ES cells have been reported to uni-directionally differentiate into neurons via NSS without selective apoptosis of non-neuronal cells using TUNEL assays [13]. Caspase 3 has been reported to be involved in differentiation from neural progenitor cells to neurons in the absence of apoptosis [51]. The metabolic pathways search also suggested that considerable axon guidance proteins, including CRMP2, were readied for the development of growth cones, and axon attraction and repulsion in NS cells (Supplementary Fig. 2F), whereas in Day 4 cells axon guidance proteins were not quite readied though CRMP2 expression was primed (Supplementary Fig. 2E). In NS cells, histone deacetylase 1 was suggested to be related to Notch signaling pathway to Hes1/5 as its co-repressor to repress differentiation to neurons (Supplementary Fig. 2G), which agreed with previously reported experiments [52]. Moreover, the metabolic pathway search suggested that regulation of the actin cytoskeleton linked to focal adhesion was related to differentiation of NS cells to AstP cells (Supplementary Fig. 2H and I). It has been reported that focal adhesion kinase mediates astrocytic actin reorganization induced by endothelin-1 [53]. Additional studies are needed to identify the pathways suggested here.

Further application of proteomics to the detailed stages of differentiation of primate ES cells, including human ES cells, into astrocytes may provide a more complete picture of primate astrocytogenesis.

## 5. Conclusions

We differentiated monkey ES cells into AstP cells *via* Day 4, NSS, and NS cells, and identified 66 differentially regulated proteins involved in these five differentiation stages using a 2-DE-based proteomic approach. Particularly, CRMP2, its phosphorylated forms, and CRABP1 were upregulated from ES cells to Day 4 and NSS cells, to which differentiation stages apoptosis-associated proteins such as caspases were possibly related. Phosphorylated CRMP2s were further upregulated but CRABP1 was downregulated from NSS cells to NS cells, during which differentiation stage considerable axon guidance proteins for development of growth cones, axon attraction, and repulsion were possibly readied. Nonphosphorylated CRMP2 was downregulated but CRABP1 was re-upregulated from NS cells to AstP cells, in which differentiation stage reorganization of actin cytoskeleton linked to focal adhesion was possibly accompanied. These results provide insight into the molecular basis of early astrocytogenesis in monkey.

Supplementary data to this article can be found online at http://dx.doi.org/10.1016/j.bbapap.2012.12.002.